Journal of Geochemical Exploration 154 (2015) 32–48

Contents lists available at ScienceDirect

Journal of Geochemical Exploration

journal homepage: www.elsevier.com/locate/jgeoexp

Concentration and distribution of mercury in drainage catchment sediment and alluvial soil of China

Xueqiu Wang [a,b,c,*], Xuemin Liu [a,d], Zhixuan Han [a,b,c], Jian Zhou [a,b,c], Shanfa Xu [a,b,c], Qin Zhang [a,b,c], Haijie Chen [a,b], Wei Bo [a,b], Xing Xia [a,b]

[a] Institute of Geophysical and Geochemical Exploration (IGGE), Chinese Academy of Geological Sciences (CAGS), Langfang, Hebei 065000, China
[b] Key Laboratory of Geochemical Exploration, Ministry of Land and Resources of PR China, China
[c] International Centre on Global-scale Geochemistry (ICGG), Langfang, Hebei 065000, China
[d] Chengdu University of Technology, Chengdu, Sichuan 610059, China

ARTICLE INFO

Article history:
Received 18 May 2014
Revised 15 January 2015
Accepted 28 January 2015
Available online 7 February 2015

Keywords:
Mercury
Geochemical baselines
Catchment sediment
Soil
China

ABSTRACT

The China Geochemical Baselines (CGB) project provides nation-wide catchment sediment/alluvial soil geochemical baseline data for 76 elements including Hg from 3382 top (0–25 cm) and 3380 deep sediment/alluvial soil samples (under a depth of 100 cm) at 3382 sampling sites, corresponding to a sampling density of about 1 site per 3000 km^2. Mercury was determined by cold vapour generation atomic fluorescence spectrometry (AFS) under strict quality control using field duplicates, standard reference materials and analytical replicate samples. The 25th percentile is at 13 and 11 μg/kg in top and deep sediment/alluvial soil samples, respectively; these concentrations are close to the crustal abundance in China. The median Hg value is at 26 and 18 μg/kg in top and deep sediment/alluvial soil samples, respectively; the 75th percentile is 56 μg/kg in top and 36 μg/kg in deep sediment/alluvial soil samples. Mercury concentrations at the 50th (26 μg Hg/kg) and 75th (56 μg Hg/kg) percentiles exhibit systematic enrichment in the near-surface material. The Hg distribution maps show distinct increasing trends from northern to southern and from western to eastern China, which are primarily related to the distribution of parent rocks, including rocks associated with mineral resources of Hg, Sb, Au, As, Pb–Zn, and climate, resulting in different soil types, as well as to population density with accompanying industrial development. Anomalous Hg concentrations in top sediment/alluvial soil samples above the 85th percentile (87 μg/kg) occur mainly in south and south-west and sparsely in north and east China; they most likely have a dual origin, natural and human-induced, with the latter having a greater contribution because of the intense industrial activities, and particularly mercury emissions from Hg, Sb, As, Au, Pb–Zn mining, coal combustion, and production of batteries, fluorescent lamps, thermometers and cement. The spatial distribution map of Hg ratios of top to deep sediment/alluvial soil samples displays higher values, suggesting that top samples are most likely polluted from human activities in the highly populated urban areas of eastern China. About 6.86% and 3.52% of top and deep sediment/alluvial soil samples, respectively, have Hg concentrations higher than the soil contamination limit of 150 μg/kg set by the National Environmental Standards for Heavy Metals of the People's Republic of China.

1. Introduction

Mercury (Hg) is a very rare chalcophile element that is found in the lithosphere, pedosphere, hydrosphere, atmosphere and biosphere (Fitzgerard and Lamborg, 2003, 2014). Mercury is one of the most toxic heavy metals and can affect the human nervous system and harm the brain, heart, kidneys, lungs, and immune system (USEPA, 1997). Widespread public concern has been focused on the toxic effects of Hg on human health since the emergence of 'Minamata disease', which is severe neuropathy caused by the consumption of methyl mercury-contaminated seafood, first observed in Minamata, Japan (Japan Environmental Agency, 1989).

Soil is considered to be the 'skin of the earth' with interfaces between the lithosphere, hydrosphere, atmosphere, and biosphere. Thus, understanding the distribution of Hg in soil is crucial for the recognition and quantification of future human-induced or natural changes in Hg concentrations that may occur in the Earth's near-surface environment.

* Corresponding author at: Institute of Geophysical and Geochemical Exploration (IGGE), Chinese Academy of Geological Sciences (CAGS), Langfang, Hebei 065000, China. Tel.: +86 316 2267629.
E-mail address: wangxueqiu@igge.cn (X. Wang).

http://dx.doi.org/10.1016/j.gexplo.2015.01.008
0375-6742/

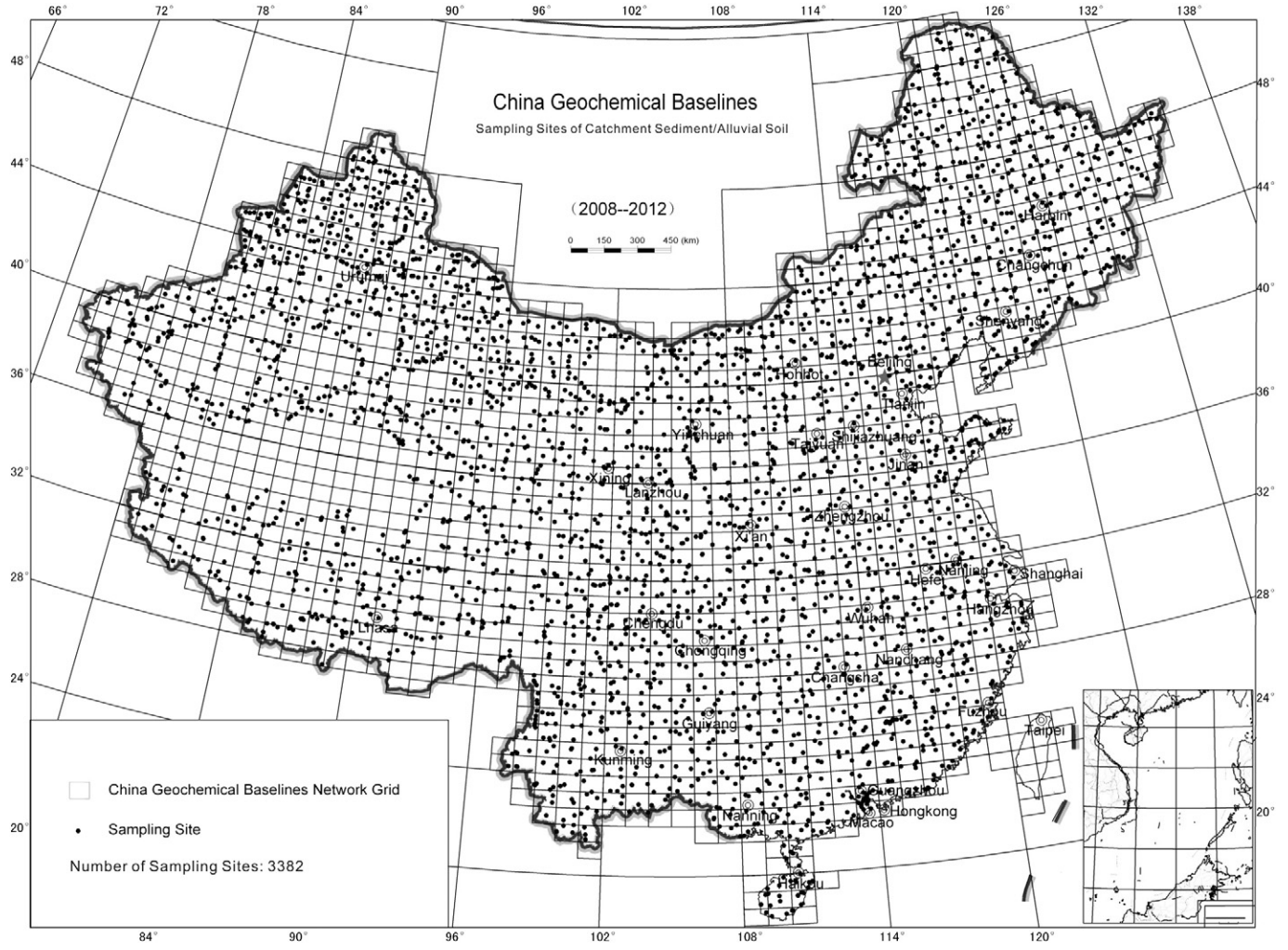

Fig. 1. Sample sites map of the China Geochemical Baselines (CGB) project.

The China Geochemical Baselines (CGB) project (Wang, 2012; Wang et al., 2010; Wang and the CGB Sampling Team, 2015), as a project of the Sinoprobe Programme (Dong and Li, 2009), was implemented from 2008 to 2013. The project, as a part of the International Union of Geological Sciences/International Association of GeoChemistry Task Group on Global Geochemical Baselines (Darnley et al., 1995; Smith et al., 2012), has provided an insight into the Hg distribution in the pedosphere of China. In this paper, the abundance and spatial distribution of Hg in China are presented with respect to geological tectonics, geomorphological landscapes, major drainage catchments and soil types. The relationship between Hg in soil and human activities is also discussed.

2. Methods

2.1. Sampling

The aim of the China Geochemical Baselines (CGB) project is to document the concentration and spatial distribution of nearly all naturally occurring chemical elements throughout China. The CGB sampling grid is based on 1:200 000 map sheets of 1° (long.) × 40′ (lat.), approximately equal to a quarter of one Global Reference Network (GRN) cell of 160 × 160 km (Darnley et al., 1995). Approximately 1500 CGB grid cells cover the whole of China (9.6 million km^2) (Wang, 2012; Wang

Table 1
Equations and cut-off values for accuracy and precision control (Zhang et al., 2012; Wang and the CGB Sampling Team, 2015).

	Accuracy control by standard	Precision control by standard	Precision control by laboratory replicate	Sampling error control by field duplicate
Equation	$\triangle lgC = \lvert lgCi\text{-}lgCs \rvert$	$RSD = \frac{\sqrt{\frac{\sum_{i=1}^{n}(Ci-Cs)^2}{n-1}}}{Cs} \times 100\%$	$RD\% = \lvert C1-C2 \rvert / [(C1+C2)/2] * 100\%$	$RE\% = \lvert So-Sd \rvert / [(So+Sd)/2] * 100\%$
Concentration range	Cut-off value	Cut-off value	Cut-off value	Cut-off value
$<3 \times DL$	≤0.15	≤17%	≤50%	≤50%
$>3 \times DL$	≤0.10	≤10%	≤40%	

Notation: Ci = the i determination value for the standard; Cs = standard reference value; C1 = the 1st determination value for the laboratory replicate sample; C2 = the 2nd determination value for the laboratory replicate sample; So = the determination value for the original field sample; Sd = the determination value for the field duplicate sample.

Table 2
Statistical results of quality control of Hg by standard reference materials.

Standard	Accuracy control			Precision control	
	Total N	Qualified N	Passing rate	RSD	Qualified control
GSS1	34	34	100%	4%	Qualified
GSS2	33	33	100%	2%	Qualified
GSS17	160	158	99%	11%	Qualified
GSS19	33	33	100%	4%	Qualified
GSS25	124	123	99%	7%	Qualified
GSS26	124	121	98%	8%	Qualified
GSS27	120	120	100%	7%	Qualified
Total	628	622	99%	/	Qualified

Notation: N = Number of samples.

Table 3
Quality control of Hg by laboratory replicate and field duplicate samples.

Laboratory replicates			Field duplicates		
Total N	Qualified N	Passing rate	Total N	Qualified N	Passing rate
660	635	96.2%	211	187	88.8%

Notation: N = Number of samples; Passing rate = (Qualified number of samples / total number samples) × 100%.

and the CGB Sampling Team, 2015). In each CGB grid cell, two sampling sites were selected at the mouth or the lowest point of each drainage catchment ranging in area from about 1000 to 5000 km^2, with most being 2000–3000 km^2, corresponding to a sampling density of about 1 sample site/3000 km^2. At each site, floodplain sediment/alluvial soil in plains, overbank sediment/alluvial soil in mountainous terrains, catchment basin sediment/alluvial soil in desert and Gobi desert terrains, or seasonal lake sediment in grassland terrains were taken at two depths: a top sample from 0–25 cm (excluding materials from the leaf litter layer, where present), and a deep sample collected from a depth of less than 100 cm or from the soil C-horizon, where this is developed. Each sample is composited from generally 3 pits in the layout of an equilateral triangle within a 50 m interval. Samples were generally not collected within 100 m of motorways/highways or roads, or within 2000 m of towns or cities. In total, 6402 routine samples and 211 duplicate field samples from 3382 sampling sites were collected during 2008–2012 (Fig. 1), covering about 94% of China. The sampling methods are described in detail in the paper entitled "*China Geochemical Baselines*: *Sampling Methodology*" in this issue (Wang and the CGB Sampling Team, 2015).

2.2. Laboratory analysis

Mercury analysis, particularly at the μg/kg level, is a key to the establishment of a nation-wide baseline database. In China, a highly-sensitive analytical method for Hg has been developed based on cold-vapour atomic fluorescence spectrometry (AFS) (Zhang and Zhang, 1986).

Soil and sediment (overbank, floodplain, lake) samples were air dried either in a room or under shade, not exposed to sunlight. This ensured there was no loss of Hg, which is a known volatile element. Grains of most samples are finer than <2 mm (10 mesh), because they are mainly composed of fine sand, silt and clay particles. Samples were sieved through a 2 mm (10 mesh) stainless steel screen in order to remove vegetation litter and coarse detritus of >2 mm. The samples were subsequently ground to <74 μm (200 mesh) in an agate or pure-aluminium porcelain mill for analysis.

An aliquot of 0.25 g was weighed and placed into a 25 ml test tube to which 10 ml of 1:1 aqua regia [aqua regia (1HNO_3 + 3HCl): pure water = 1:1 vol.] was added. The test tube was heated in a boiling water bath for 1 h and shaken 1 time during the course of decomposition. After cooling, 1 ml potassium permanganate solution (1%) was added into the solution and left standing for 30 min. Then the solution was diluted to 25 ml with oxalic acid solution (1%), shaken well, and then left standing until the particles settled and the supernatant solution was clear. A 5.0 ml aliquot of the solution was transferred into the hydride generator and covered with a ground-glass stopper. Then 7.0 ml of stannous chloride solution was added quantitatively to make the argon carrier gas flush the Hg vapour into the silica-tube furnace atomiser. Mercury atoms are excited resulting in a fluorescent signal and the peak is recorded by the fluorescent spectrometer. The detection limit (DL) is very low at 2 μg/kg Hg (Zhang et al., 2012).

2.3. Quality control

The quality control (QC) procedure of CGB project includes checks on field sampling and insertion of field duplicate samples, laboratory replicate samples and standard reference materials. The quality control methods are described in detail by Wang and the CGB Sampling Team (2015). This section only describes the Hg quality control results, including sampling error control by field duplicates, proportion of reportable Hg values, accuracy and precision control by standards, and precision control by laboratory replicates. Table 1 lists the equations and cut-off values for quality control. The cut-off value means the qualified limit of quality control below or above which the analytical results are considered unacceptable. For example, the cut-off value of RSD is ≤10% for precision of standard determinations, if the calculated RSD is above 10%, the analytical results are not acceptable.

In total, 6614 samples were analysed for Hg with 6612 samples having concentration values above the DL of 2 μg/kg; only 2 samples were below the DL. Therefore, the proportion of reportable Hg values is 99.97% of the total, which meets the requirement of the project to have 90% of the total number of samples above the DL.

Seven soil standard reference materials (SRMs), GSS1, GSS2, GSS17, GSS19, GSS25, GSS26 and GSS27 (Xie et al., 1985, http://www.gbw114.org/d_120453.htm; http://www.gbw114.org/d_120461.htm), were used to monitor analytical quality. Four standards unknown to the analysts were randomly inserted into each batch of 50 samples. In total, 628 determinations on standard samples were made within the suite of 6617 samples. Accuracy and precision are tabulated in Table 2. The passing rate for accuracy is over 98% and for precision all SRMs are at 100% according to the cut-off values.

Laboratory replicates were used to control analytical precision. Five laboratory replicates unknown to the analysts were inserted into each batch of 50 samples for precision control. In total, 660 laboratory replicates were inserted into the suite of 6617 samples. The Relative Deviation (RD%) of determination values of the replicates were calculated and are tabulated in Table 3. In total, 635 replicates meet the requirement for RD less than 50% below 3xDL and 40% over 3xDL. The passing rate is 96.2% (Table 3).

Table 4A
Statistical parameters of Hg analytical results (μg/kg) in top and deep sediment/alluvial soil samples from the CGB project.

Sample type	N	DL	Min.	P2.5	P25	P50	P75	P85	P97.5	Max.	Mean	Geometric Mean
Top	3382	2	<2	5.2	13.1	26.0	55.5	86.9	279	20,201	67.0	28.7
Deep	3380	2	<2	4.6	10.5	18.0	36	55.2	188	60,001	64.8	21.0

Notation: N = Number of samples; DL = Detection Limit; P = Percentile (P50 = median); Min. = Minimum; Max. = Maximum.

Table 4B
Statistical parameters of Hg analytical results (μg/kg) in top sediment/alluvial soil samples from the CGB project, used for map plotting. For comparison purposes the Hg concentrations are the same except, of course, the maximum value, as those of the deep sediment/alluvial soil samples.

Sample type	N	DL	Min.	P1.2	P17.2	P36.1	P61.7	P74.7	P95.2	Max.	Mean	Geometric mean
Top	3380	2	<2	4.6	10.5	18.0	36	55.2	188	60,001	64.8	21.0

Field duplicate samples were taken to control field sampling errors. A total of 211 field duplicate samples (109 top and 113 deep samples) from 113 control sites were collected. The relative sampling error (RE%) was calculated based on the pairs after laboratory analysis. The relative error of 187 duplicates is less than 50%. The passing rate is 88.8% (Table 3).

3. Results and discussion

3.1. Concentration of mercury in China

Tables 4A and 4B show the statistical summary for Hg concentrations in top and deep samples of the CGB project. The median concentration of Hg in top samples is 26 μg/kg and in deep samples 18 μg/kg. The Hg concentration at the 25th percentile (P25) is 13.1 and 10.5 μg/kg in top and deep samples, respectively. The 75th percentile (P75) of Hg concentrations is 55.5 and 36 μg/kg in top and deep samples, respectively.

Crustal abundance of Hg at n × 100 μg/kg was first estimated on 5159 igneous rocks by Clarke and Washington (1924), and subsequently reported by Parker (1967). Other, more recent, estimates are: 500 μg/kg by Goldschmidt (1954), 83 μg/kg by Vinogradov (1962), 80 μg/kg by Taylor (1964), 96 μg/kg by Shaw et al. (1986), and 40 μg/kg by Wedepohl (1995). All values estimated before the 1990s may be higher than the true crustal average due to lack of analytical methods for Hg with a low detection limit. After the 1990s, the crustal abundance of Hg in China was estimated at 7 μg/kg by Yan and Chi (1997) and by Chi and Yan (2007), and 9 μg/kg by Gao et al. (1999). While Gao et al. (1998) give the following continental crust estimates for Hg from their studies in Eastern China by using an atomic fluorescence analytical method with a detection limit of 2 μg/kg: 9.4 μg/kg interior of the North China craton, 8.1 μg/kg southern margin of the

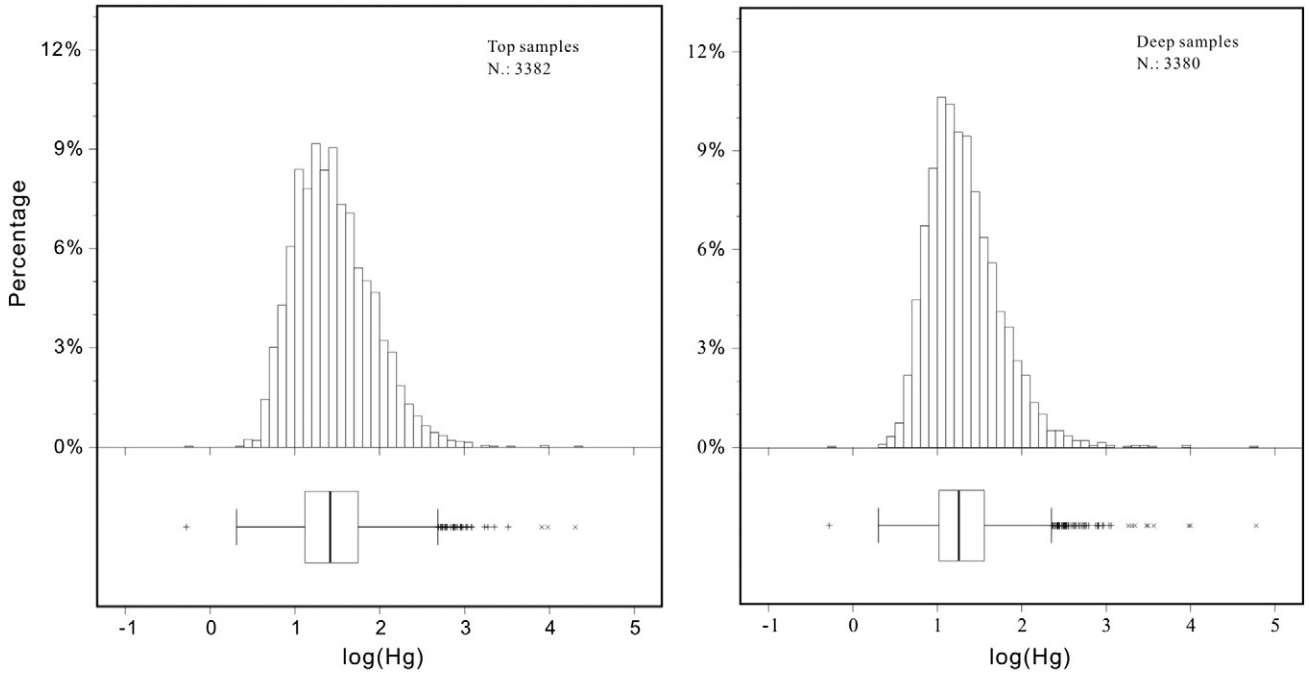

Fig. 2. Histograms and boxplots displaying the statistical Hg (μg/kg) distribution in top and deep sediment/alluvial soil samples of CGB project results. Box length represents the interquartile range (25th to 75th percentiles) and contains the median (thick black line). "+": cases with values between 1.5 and 3 times box length (interquartile range) from the lower or upper edge of the box; "×": cases with values more than 3 times box length from the lower or upper edge of the box (Kürzl, 1988; Tukey, 1977).

Table 5
Proportion of top and deep sediment/alluvial soil samples out of total sampling locations exceeding the limit of 150 μg/kg Hg according to the China National Environmental Standards for Heavy Metals (GB 15618-1995).

Sample type	Total N	<150 μg/kg		150–500 μg/kg		500–1500 μg/kg		>1500 μg/kg	
		Clean		Slight exceedance		Medium exceedance		High exceedance	
		N	Proportion	N	Proportion	N	Proportion	N	Proportion
Top	3382	3150	93.14%	195	5.77%	30	0.89%	7	0.21%
Deep	3380	3261	96.48%	94	2.78%	16	0.47%	9	0.27%

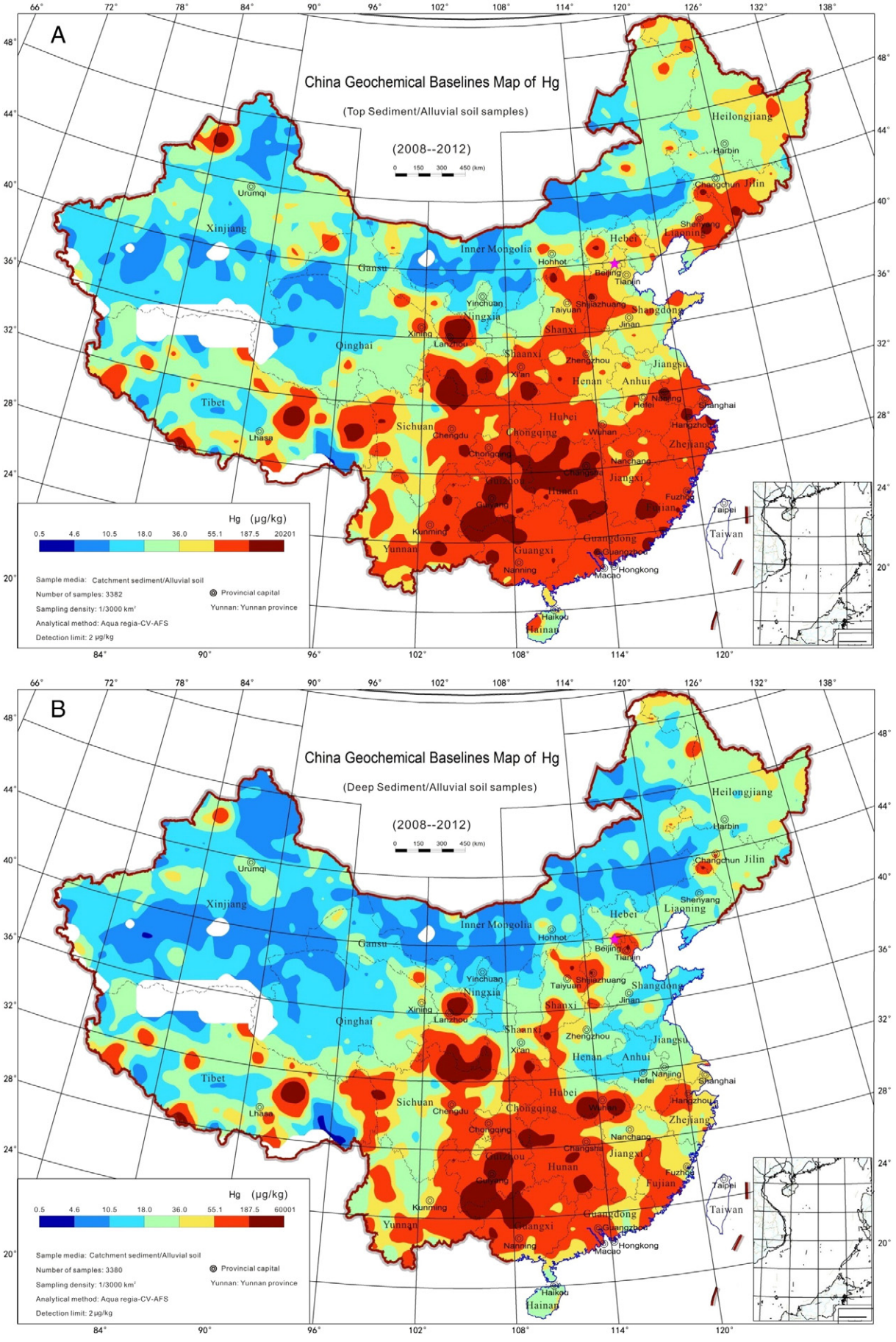

Fig. 3. Mercury distribution map in top (A) and deep (B) sediment/alluvial soil samples from the CGB project.

North China craton, 24.2 μg/kg North Qinling belt, 26.6 μg/kg South Qinling belt, 10.8 μg/kg Yangtze craton and 11.5 μg/kg central East China as a whole, showing that there is significant variation in Eastern China. From these studies, it appears that the continental crust estimate for Hg in China varies from 7 to 11.5 μg/kg, not taking into account the two high values in North and South Quinling belt. The 25th percentile values, determined in this study (13 μg/kg in top and 11 μg/kg in deep samples), are close to the estimated crustal abundance of China. The median (P50) Hg values, both in top (26 μg/kg) and deep (18 μg/kg) samples, are greatly elevated compared to the estimated crustal abundance of China.

Table 4A clearly shows that the Hg concentrations <P25 are very similar for both top and deep samples (ratio top/deep samples: 1.18), whereas Hg values in the top samples at percentiles greater than the median (>P50) have distinctly higher concentrations than the corresponding deep samples, as indicated by Top/Deep sample ratios at the 50th, 75th, 85th and 97.5th percentiles of 1.44, 1.56, 1.58 and 1.49, respectively, suggesting an enrichment. For comparison purposes, the same Hg concentrations in top sediment/alluvial soil samples are used for map plotting as those of the deep samples (Table 4B). Fig. 2 presents the Hg statistical distribution of top and deep samples in the form of histograms and boxplots. The boxplots indicate the presence of a limited number of lower outliers, while there is a considerable number of upper outliers. This aforementioned statistical information shows that there is no, or only a small, difference between top and deep samples at low concentrations, and there are large difference at high concentrations and systematic enrichment in top samples until the 97.5th percentile.

Table 5 lists the proportion of sample sites relative to total sampling locations that exceed the limit value of 150 μg Hg/kg set by the National Environmental Standards for Heavy Metals of the People's Republic of China (GB 15618-1995). Therefore, the proportion of top and deep sediment/alluvial soil samples exceeding the Chinese statutory limit of 150 μg/kg Hg is 6.87% and 3.52%, respectively.

3.2. General distribution of mercury throughout China

The spatial distribution of Hg throughout China is shown on the contoured geochemical maps (Fig. 3). The maps were produced from gridded data, which were processed by the in-house software Geoexpl2009® (http://www.drc.cgs.gov.cn/GeoExplGeoMDlS/). Raw analytical data were interpolated to generate a regular output grid of 80 × 80 km, using an exponentially weighted moving average model. The 18-shade colour mapped classes are based on the following percentiles of raw data: 2.5, 5, 10, 15, 20, 25, 30, 40, 50, 60, 70, 75, 80, 85, 90, 95 and 97.5. The different colour shades given to percentiles at 2.5 (dark blue), 25 (blue), 50 (green), 75 (yellow), 85 (red) and 97.5 (dark red) were selected to make easier the reading and interpretation of the Hg and organic carbon distribution maps (Figs. 3 & 4).

The most noticeable Hg distribution pattern shown on the maps of both top and deep samples is the trend of increasing concentrations from north to south and from west to east. The distribution patterns

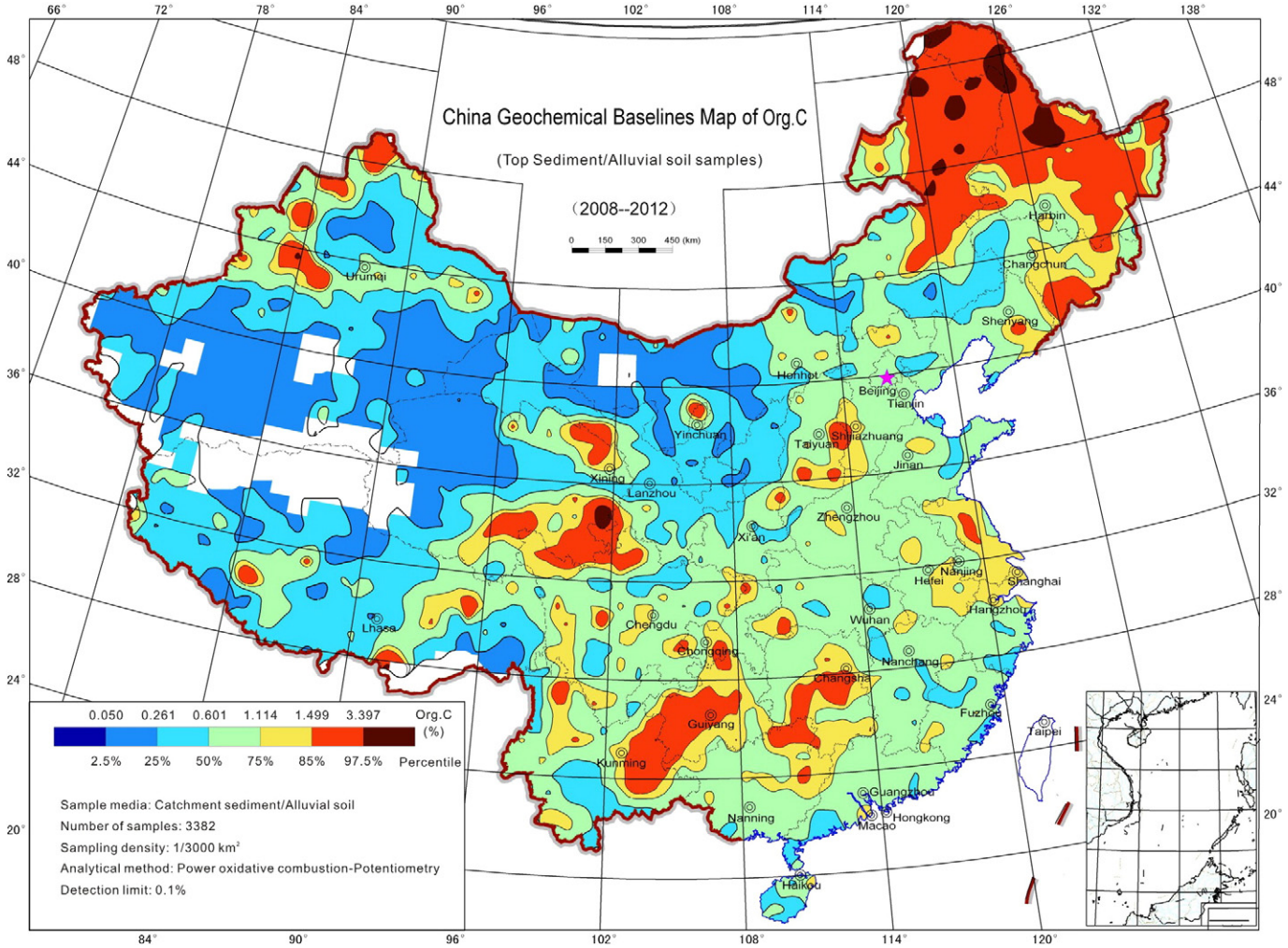

Fig. 4. Organic carbon distribution map in top sediment/alluvial soil samples from the CGB project.

are related to (1) parent rocks, including rocks associated with mineralisation; (2) climate, which is a major factor in forming the major soil types of China; and (3) human activities.

Low Hg concentrations (<P25, blue colours) are distributed in arid desert basins, Gobi desert, semi-desert grassland and loess in the north and north-west of China, where the sediment/soil is comprised mostly of quartz-rich windblown sand containing low content of organic matter and is unpolluted or only slightly polluted by human activities.

High Hg concentrations (P75-P85, yellow-orange colours) are correlated with lithology, such as black shale of Lower Cambrian Formation of Yangtze Craton, as discussed in a later section (Mao et al., 2002), with red earth and laterite in southern China, and with soil containing high content of organic matter in north-eastern China (Fig. 4).

Mercury anomalies (threshold is here defined as >P85, red colours) both in top and deep samples are distributed in south and south-west parts of China. The largest one covers Hunan, Guizhou, Chongqin, East Yunnan, North Guangxi, and south-east Sichuan, where large-scale low-temperature metallogenic provinces occur that are characterised by mineralisation of Hg, Sb, As, Au, P, Pb–Zn, Ni–Mo-PGEs, baryte and calcite (Coveney and Chen, 1991; Hu et al., 2002, 2007; Huang et al., 2011).

Mercury anomalous centres (>P97.5, dark red) are exactly correlated with Hg mineralisation and low-temperature mineral deposits. For example, the top and deep samples with maximum Hg concentrations of 20,201 and 60,001 μg/kg, respectively, were taken from the same site, which is located at the lower reaches of the Lannigou gold deposit (Hu et al., 2002) and the Lanmuchang Hg deposit in Guizhou (Qiu et al., 2006). Other areas of high Hg in top samples sparsely occurring at the border area of Sichuan, Shaanxi and Gansu provinces, in eastern Shandong, in Hebei, in eastern Jilin and Liaoning are due to the largest gold-producing districts in China, where artisanal gold smelting with Hg amalgamation was used (Gunson and Viega, 2004; Gunson and Yue, 2001). In September 1996, this practice was officially banned in China, because of potential Hg pollution (Lin et al., 1997).

The area of high anomalous Hg concentrations (>P97.5) in top samples is larger in extent than that in deep samples. According to applied geochemists' experiences on the interpretation of floodplain sediment/alluvial soil geochemical maps (e.g., De Vos et al., 2006; Ottesen et al., 2013) (1) spatial distribution patterns based on deep sediment/alluvial soil samples are usually related to lithology/mineralisation, and may designate the geochemical background for top sediment/alluvial soil, and also may indicate the influence of human activities in regions with a high-degree of industrialisation or long-history of mining and smelting; (2) the geochemical patterns based on top samples are related to both lithology/mineralisation, and human activities, and (3) the distribution map of top/deep sediment/alluvial soil ratio depicts, in most cases, the superimposed anthropogenic influence.

The spatial distribution map of Hg ratios of top to deep samples better visualises the possible impact from human activities on top sediment/alluvial soil in the highly populated urban areas of eastern China and mining districts (Fig. 5). For example, a significant anomaly of Hg ratios of top to deep samples occurs at the lower reaches of the

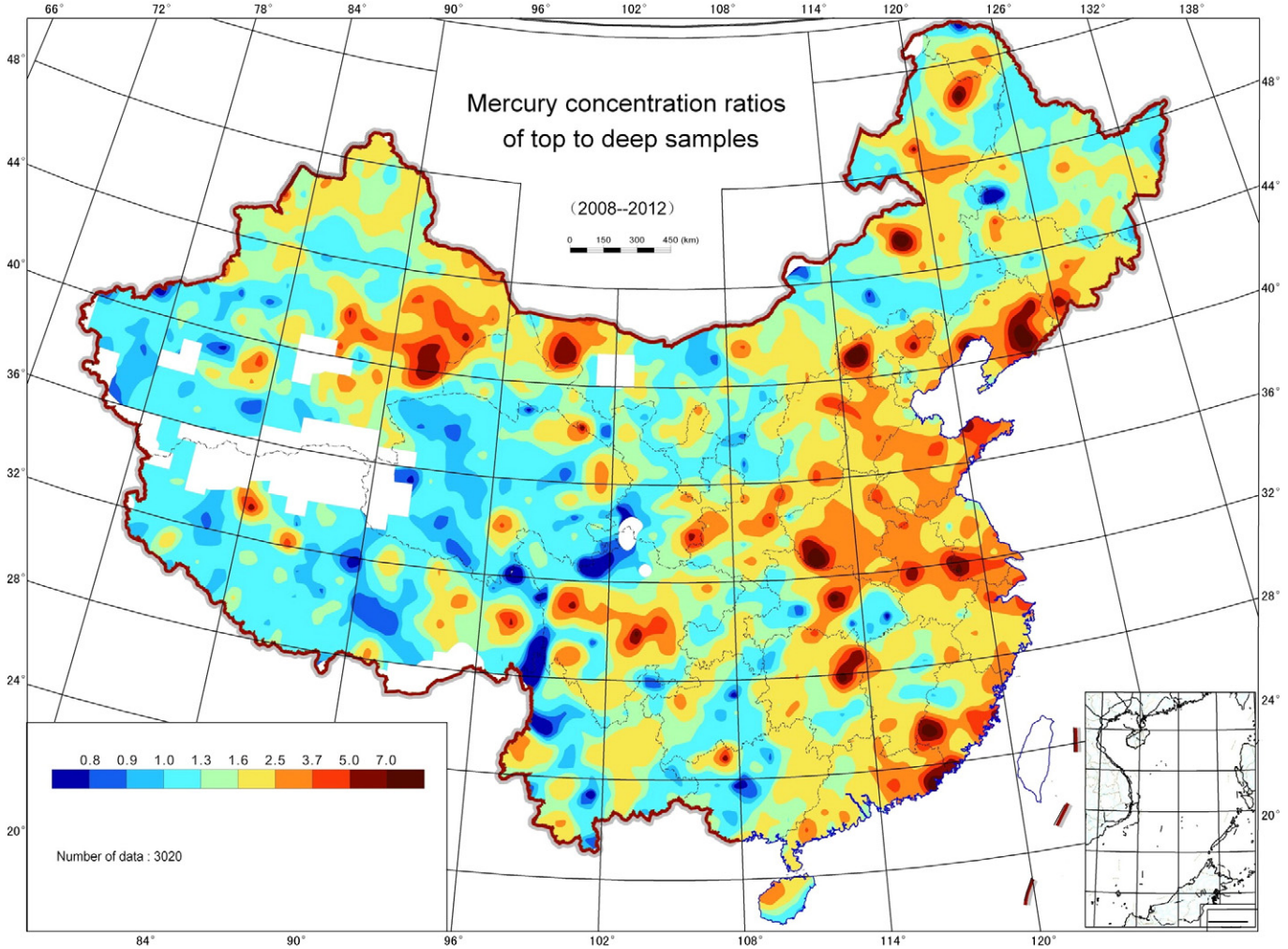

Fig. 5. Distribution map of Hg concentration ratios of top to deep sediment/alluvial soil samples from the CGB project.

Fig. 6. Tectonic units of China (redrawn from Ren et al., 1999, Fig. 6, p.12).

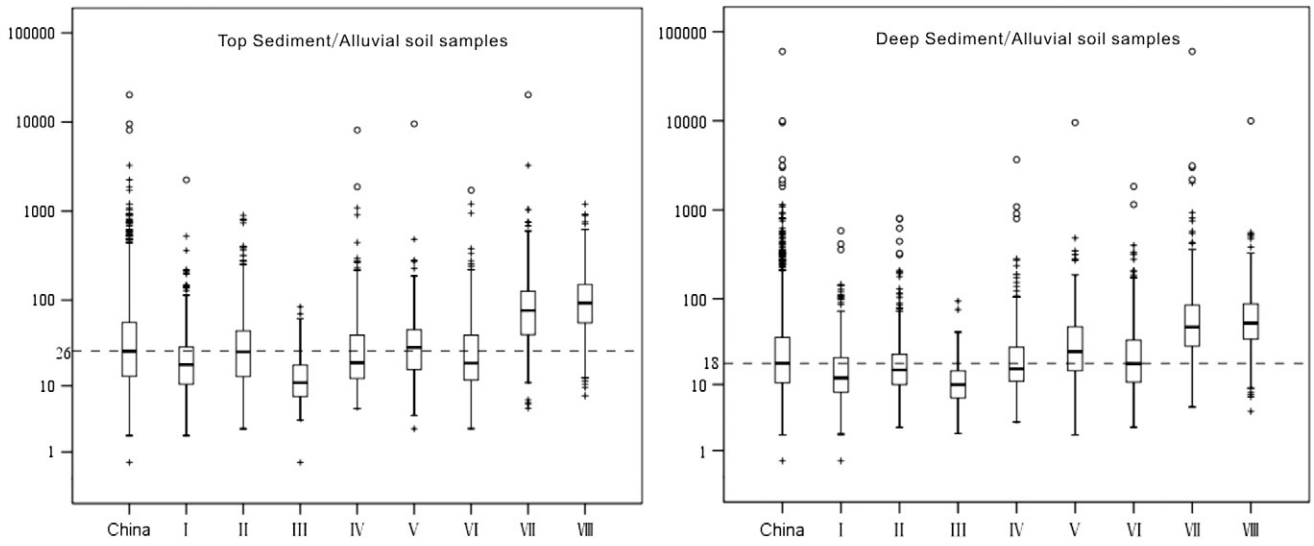

Fig. 7. Boxplots showing the Hg (μg/kg) variation in top and deep sediment/alluvial soil samples in different tectonic units of China (for summary statistics refer to Table 6). The dotted lines at 26 and 18 μg/kg Hg mark median concentrations of top and deep sediment/alluvial soil samples in whole China, respectively. Box length represents the interquartile range (25th to 75th percentiles) and contains the median (thick black line). "+": cases with values between 1.5 and 3 times box length (interquartile range) from the upper or lower edge of the box; "": cases with values more than 3 times box length from the lower or upper edge of the box (Kürzl, 1988; Tukey, 1977). Notation: China — All samples; (I) Tianshan–Xingmeng Orogenic Belt; (II) North China Craton; (III) Tarim Craton; (IV) Qin–Qi–Kun Orogenic Belt; (V) Songpan–Ganzi Orogenic Belt; (VI) Tibet–Sanjiang Orogenic Belt; (VII) Yangtze Craton.

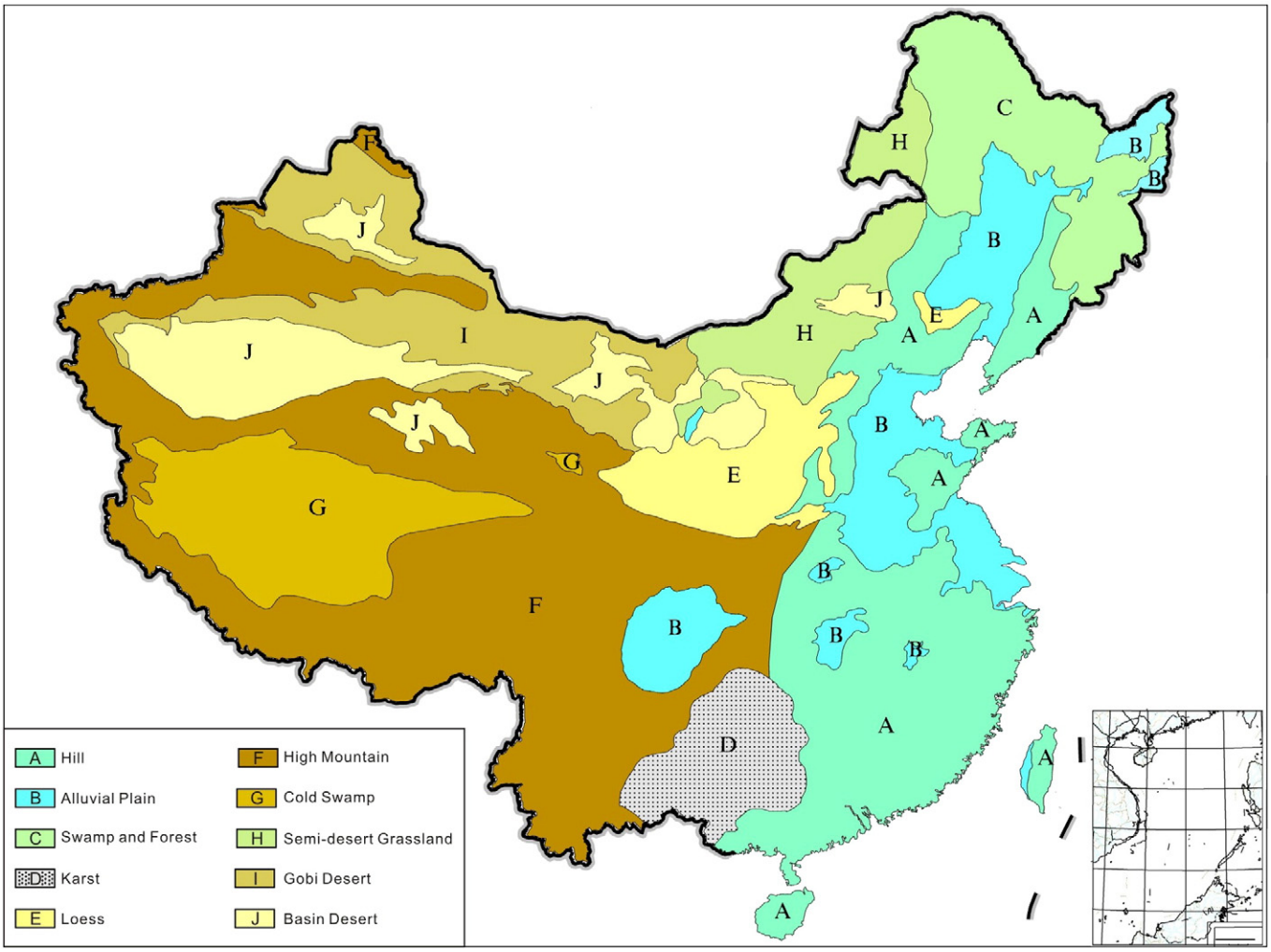

Fig. 8. China's geomorphological landscape terrains.
Modified from Wang and Zuo (2010).

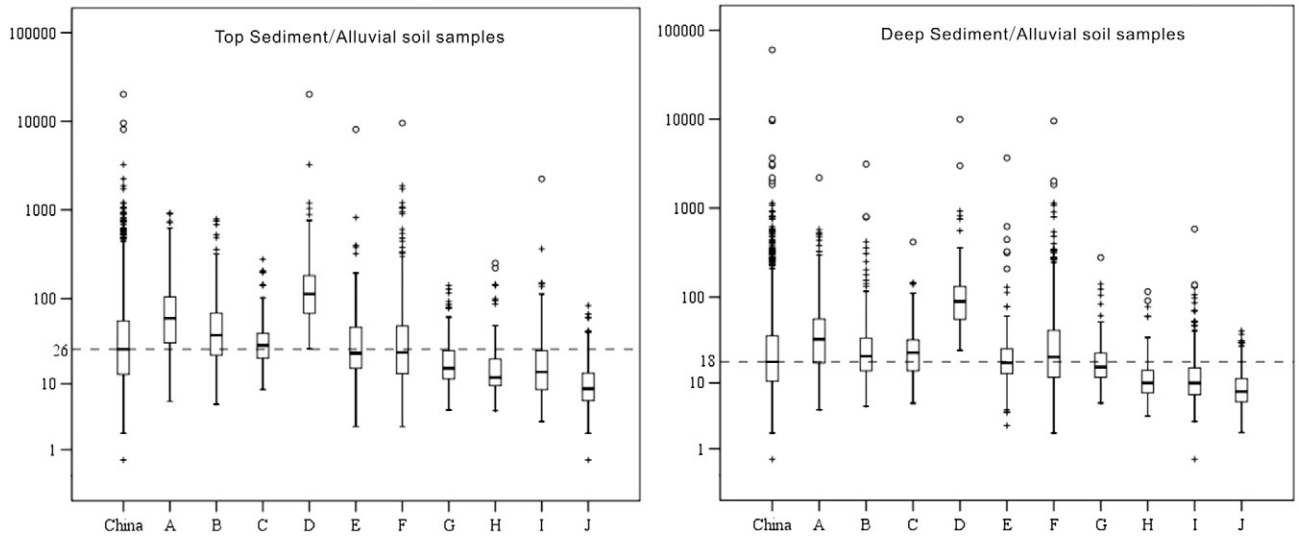

Fig. 9. Boxplots displaying statistical Hg (μg/kg) variation of top and deep sediment/alluvial soil samples in the different geomorphological landscape terrains of China (for boxplot characteristics see Fig. 7, and for summary statistics refer to Table 7). Notation: China — All samples; (A) Hill; (B) Alluvial Plain; (C) Swamp and Forest; (D) Karst; (E) Loess; (F) High Mountain; (G) Cold Swamp; (H) Semi-desert Grassland; (I) Gobi Desert; (J) Basin Desert.

Table 6
Statistical parameters of Hg analytical results (μg/kg) in top and deep sediment/alluvial soil samples in China's geological tectonic terranes (see also Fig. 7).

Tectonic terrane	Sample type	N	Percentile								Mean	Geometric mean
			Min.	2.5%	25%	50%	75%	85%	97.5%	Max.		
Whole China	Top	3382	0.5	5.2	13.1	26.0	55.5	86.9	279	20,201	67.0	28.7
	Deep	3380	0.5	4.6	10.5	18.0	36.0	55.2	188	60,001	64.8	21.0
Orogenic Belts (OB, all)	Top	2160	2.0	5.2	12.9	23.5	48.8	79.9	270	9550	60.0	26.9
	Deep	2158	0.5	4.5	10.2	17.5	36.0	54.0	185	9976	47.1	20.5
Cratons (all)	Top	1222	0.5	5.2	14.0	30.5	68.0	97.2	319	20,201	79.5	32.2
	Deep	1222	2.1	4.7	11.0	19.0	36.5	59.1	207	60,001	96.1	21.9
Tianshan–Xingmeng Orogenic Belt (I)	Top	909	2.0	5.1	10.5	18.0	29.0	38.2	85.9	2246	27.5	18.5
	Deep	907	0.5	4.0	8.0	12.1	21.0	28.0	64.7	583	18.7	13.3
North China Craton (II)	Top	613	2.6	5.5	13.0	25.5	44.5	63.0	216	901	44.6	26.0
	Deep	613	2.6	5.0	10.0	15.0	23.0	28.5	82.5	802	24.9	15.8
Tarim Craton (III)	Top	209	0.5	4.1	7.3	11.0	17.8	22.6	43.7	83.4	14.7	11.7
	Deep	209	2.1	3.8	6.8	9.9	14.6	18.4	37.5	93.9	12.5	10.3
Qin–Qi–Kun OB (IV)	Top	350	5.1	6.1	12.3	19.0	39.7	59.0	240	8125	68.6	23.5
	Deep	350	3.2	5.1	11.0	15.5	27.7	39.0	177	3670	44.3	18.7
Songpan–Ganzi OB (V)	Top	202	2.6	5.8	15.9	28.7	45.8	68.7	187	9550	90.0	29.6
	Deep	202	2.0	5.7	14.8	24.8	48.0	66.0	269	9550	90.6	28.3
Tibet–Sanjiang OB (VI)	Top	349	2.7	4.6	11.7	18.8	39.9	64.7	198	1720	46.5	22.7
	Deep	349	2.7	4.5	10.7	17.8	33.6	52.0	190	1835	41.6	20.5
Yangtze Craton (VII)	Top	400	5.1	18.0	40.3	76.0	125	172	497	20,201	167	74.9
	Deep	400	5.1	14.0	28.7	47.0	84.0	111	419	60,001	249	52.4
South China OB (VIII)	Top	350	7.5	17.9	55.0	92.5	151	202	592	1201	132	93.0
	Deep	350	4.5	11.8	34.5	52.5	88.3	122	306	9976	104	57.9

Baiyindaba Pb–Zn–Ag mine in Inner Mongolia (Fig. 5, 118°E, 45°N), which has been mined since 2006, and in the area there are also coal mines in operation since 2000. The top soil samples are contaminated, whereas the deep sediment/alluvial soil samples are not impacted by mining activities.

It was estimated that Hg emission from non-ferrous metal smelting, coal combustion and miscellaneous uses (e.g., battery, fluorescent lamp, thermometer, and cement production) contributed about 45%, 38% and 17%, respectively, based on official statistical data of Hg emissions from anthropogenic activities in China for 1999 (Streets et al., 2005; Wang and Zuo, 2010; Wu et al., 2006; Zhang and Wong, 2007).

3.3. Mercury distribution in relation to China's tectonic framework

Mainland China is geologically divided into eight tectonic units (Fig. 6): (I) Tianshan–Xingmeng Orogenic Belt, (II) North China Craton, (III) Tarim Craton, (IV) Qin–Qi–Kun Orogenic Belt, (V) Songpan–Ganzi Orogenic Belt, (VI) Tibet–Sanjiang Orogenic Belt, (VII) Yangtze Craton and (VIII) South China Orogenic Belt (Fig. 6) (Ren et al., 1999). The continental crust of China is a mosaic of cratonic blocks and orogenic belts, containing small cratons and terranes with various tectonic settings (Zheng et al., 2013). The Tianshan–Xingmeng Orogenic Belt (I), also known as part of the Central Asian Orogenic Belt (CAOB) or the Altaid tectonic collage (Şengör et al., 1993), lies between the Siberian craton to the north, and the Tarim and North China cratons to the south, and is characterised by huge volumes of volcanic rocks and granite masses (Miao et al., 2007; Wu et al., 2001, 2007; Zhang et al., 2008, 2010). The North China Craton (NCC) (II) is one of the world's oldest Archaean cratons. The basement rocks of the East NCC are exposed as high- or low-grade granite-greenstone, which is dominated by Archaean granitic gneiss and tonalitic–trondhjemitic–granodioritic (TTG) gneiss, while the western NCC is mostly covered by the Ordos Basin (Li, 2012; Zhao

Table 7
Statistical parameters of Hg analytical results (μg/kg) in top and deep sediment/alluvial soil samples in China's diverse geomorphological landscapes (see also Fig. 9).

Geomorphological landscape	Sample type	N	Percentile								Mean	Geometric Mean
			Min.	2.5%	25%	50%	75%	85%	97.5%	Max.		
Whole China	Top	3382	0.5	5.2	13.1	26.0	55.5	86.9	279	20,201	67.0	28.7
	Deep	3380	0.5	4.6	10.5	18.0	36.0	55.2	188	60,001	64.8	21.0
Hill (A)	Top	633	6.0	9.0	31.0	59.5	105	152	407	921	93.7	59.7
	Deep	633	4.5	6.5	17.5	33.1	56.5	78.1	211	2191	53.5	33.3
Alluvial plain (B)	Top	335	5.5	6.5	22.3	38.0	68.3	90.0	287	794	62.3	38.5
	Deep	335	5.0	6.5	14.0	21.0	34.0	47.0	169	3121	46.0	23.5
Swamp and forest (C)	Top	218	8.5	12.2	20.5	29.0	39.9	45.5	124	278	36.1	29.9
	Deep	217	5.5	6.4	14.0	23.0	32.5	38.8	69.2	416	27.8	21.6
Karst (D)	Top	126	26.5	31.6	68.0	113	180	230	1018	20,201	348	122
	Deep	126	24.5	28.3	56.3	89.5	132	190	917	60,001	701	104
Loess (E)	Top	170	2.6	7.6	15.5	23.5	46.3	63.2	291	8125	93.0	28.4
	Deep	170	2.6	5.1	13.1	17.5	25.5	32.8	290	3670	53.7	20.3
High mountain (F)	Top	923	2.6	5.2	13.4	24.0	48.5	75.0	254	9550	62.8	27.4
	Deep	923	2.0	4.6	11.7	20.5	41.8	65.3	207	9550	56.4	23.5
Cold swamp (G)	Top	140	4.6	6.1	11.6	15.6	25.0	29.3	89.7	141	22.8	17.6
	Deep	140	5.5	6.6	11.7	15.6	22.7	25.7	94.7	277	21.9	16.6
Semi-desert grassland (H)	Top	215	4.5	5.5	9.5	12.0	20.0	25.0	92.2	251	19.3	14.1
	Deep	214	3.6	4.5	7.5	10.0	14.2	18.0	34.0	116	13.1	10.8
Gobi desert (I)	Top	424	3.1	4.9	8.5	14.0	25.1	34.7	84.6	2246	26.7	15.4
	Deep	424	0.5	3.6	7.1	10.0	15.2	18.7	49.0	583	15.0	10.8
Basin desert (J)	Top	198	0.5	3.6	6.1	8.7	13.5	16.9	42.4	83.4	11.8	9.3
	Deep	198	2.0	3.6	5.8	7.8	11.3	15.2	30.0	41.4	9.9	8.4

et al., 2003). The Tarim Craton (III) is the largest sedimentary basin in China with an area of about 560,000 km^2. The Palaeozoic sequence comprises mainly dolomitic limestone and red and yellow siltstone, while the Mesozoic and Caenozoic strata consist mainly of green sandstone and red mudstone. The Qin–Qi–Kun Orogenic Belt (IV) stretches approximately E–W from Jiaodong peninsula in the east to the south-western margin of the Tarim Block in the west (Pirajno, 2013). The eastern part is the world's largest ultrahigh pressure (UHP) metamorphic belt, consisting of gneiss, granulite and migmatite, and the lithostratigraphical sequence is made up from mostly Devonian–Cretaceous sedimentary rocks with widespread granitic masses formed in the Triassic. The basement of the western part consists mainly of amphibolite facies gneiss, schist and migmatite, overlain by a sedimentary sequence, which is locally intruded by gneissic potassic granite (Song et al., 2006; Wang, 2004; Xu et al., 1996). The Songpan–Ganzi Orogenic Belt (V) contains turbidity sediments from 5 to 15 km thick, representing the largest volume of flysch facies in the world (Pirajno, 2013; Wang et al., 2008). The lithostratigraphy comprises mostly Triassic deep marine sedimentary limestone, calcareous shale, sandstone, siltstone and turbiditic clastic rocks. Except for some Triassic granite masses, Na-rich and peraluminous rhyolite and high MgO andesite in the northern Songpan–Ganzi terrane near the suture between the Songpan–Ganzi and Kunlun terranes are the only known coeval volcanic rocks (Pirajno, 2013; Wang et al., 2008). The Tibet–Sanjiang Orogenic Belt, also known as the Tibetan Plateau (VI), is commonly considered to be the product of the India–Asia collision starting in the early Caenozoic (Zhu et al., 2013). The sedimentary sequences are characterised by dominantly shallow marine clastic sediments and carbonate rocks, fluvial sedimentary sequences, and volcanic flows (Kapp et al., 2003). The intrusions comprise granitoids, ultramafic rocks and volcanic rocks (Harris et al., 1988, 1990; Kapp et al., 2003; Pirajno, 2013; Xu et al., 1985; Yin and Harrison, 2000). The Yangtze Craton (VII) consists of minor Archaean–Palaeoproterozoic crystalline basement, and the Palaeozoic strata are primarily composed of marine carbonates and clastic sediments, with limited magmatism. The Lower Cambrian black shale in the Yangtze craton sedimentary sequence extends along a belt 1600 km long, from Yunnan Province in the south-southwest to Zhejiang Province in the central-east. Basalt at Emeishan in Sichuan Province occurs in the western margin of the Yangtze Craton (Xu et al., 2004; Zheng et al., 2013). The South China Orogenic Belt (VIII) in the south-east is characterised by widespread intrusive and volcanic rocks of Yanshanian age (Mesozoic), forming a magmatic belt extending for more than 400 km from Hainan Island to Zhejiang Province to the north-east (Pirajno, 2013).

Table 7 shows the statistical results of Hg concentrations in top and deep soil samples in different tectonic terranes of China, and Fig. 9 the statistical distribution in the form of boxplots. The median in top samples is 23.5 μg/kg in orogenic belts and 30.5 μg/kg in cratons, and

Fig. 10. Major river basins of China.
Modified from Wang and Zuo (2010).

the corresponding values in deep samples are 17.5 and 19 μg/kg, respectively. The boxplots (Fig. 9) indicate the presence of a limited number of lower outliers for top and deep samples, while there is a considerable number of upper outliers. The highest Hg median value in deep samples at 77 μg/kg is in Yangtze Craton (Fig. 6, VII; Table 6) where black shale is widely distributed and Hg, low-temperature gold and base metal deposits occur. The lowest Hg median value for both top and bottom samples is in the Tarim Craton (Fig. 6, III; Table 6) due to sandstone

Table 8
Statistical parameters of Hg analytical results (μg/kg) in top and deep sediment/alluvial soil samples in the 32 major drainage basins of China (see also Fig. 11).

Drainage Basin	Sample type	N	Percentile								Mean	Geometric Mean
			Min.	2.5%	25%	50%	75%	85%	97.5%	Max.		
Whole China	Top	3382	0.5	5.2	13.1	26.0	55.5	86.9	279	20,201	67.0	28.7
	Deep	3380	0.5	4.6	10.5	18.0	36.0	55.2	188	60,001	64.8	21.0
Yangtze River (C1)	Top	663	2.6	10.4	32.3	**67.0**	118	168	523	9550	124	64.3
	Deep	663	2.0	9.9	24.5	**42.5**	76.8	106	398	9550	101	46.2
Heilongjiang River (C2)	Top	349	5.5	8.9	18.0	26.0	36.5	42.5	110	213	32.0	26.2
	Deep	348	4.2	6.0	12.0	19.0	30.0	35.5	70.7	416	25.1	19.4
Yellow River (C3)	Top	306	2.6	5.8	15.1	23.3	40.2	61.1	163	8125	65.7	25.8
	Deep	306	2.6	4.6	12.0	17.5	26.9	37.6	121	3670	40.8	19.4
Pearl River (C4)	Top	134	12.5	29.2	58.9	**102**	157	202	707	20,201	291	105
	Deep	134	15.0	24.8	45.4	**72.5**	117	139	475	60,001	615	79.8
Yarlung Zangbo River (C5)	Top	111	2.7	3.5	9.9	17.8	38.1	67.4	243	1208	52.5	20.3
	Deep	111	2.7	3.5	7.8	14.3	36.6	54.6	254	1835	59.5	18.7
Haihe River (C6)	Top	102	6.5	7.9	24.8	40.0	60.8	79.2	306	901	66.7	40.5
	Deep	102	3.6	6.9	15.0	21.3	28.4	34.0	381	802	48.4	23.5
South-eastern Coast River (C7)	Top	91	18.0	29.1	54.8	**83.5**	134	196	573	921	129	93.8
	Deep	91	10.5	14.1	32.5	**43.0**	59.0	72.3	166	476	57.6	45.3
Huaihe River (C8)	Top	86	6.0	12.5	28.0	38.3	50.8	69.0	108	201	45.6	39.1
	Deep	86	4.5	6.0	13.0	15.8	20.9	26.0	55.9	195	20.9	17.3
Liaohe River (C9)	Top	83	5.5	6.0	8.3	13.0	26.3	47.2	152	739	38.0	17.3
	Deep	83	5.0	5.5	7.5	10.5	14.5	17.9	31.8	358	16.4	11.4
Lancangjiang River (C10)	Top	56	6.0	6.4	12.2	37.4	59.1	84.1	313	1720	79.4	30.9
	Deep	56	6.0	6.4	12.7	21.9	45.6	51.9	263	335	43.5	25.5
Nujiang River (C11)	Top	45	9.7	10.6	24.8	48.5	78.7	94.3	180	227	56.4	42.7
	Deep	45	9.0	9.4	22.5	48.0	76.3	103	119	173	55.4	41.9
Shandong Peninsula River (C12)	Top	39	11.2	13.4	26.0	32.5	62.3	76.5	143	404	53.1	39.2
	Deep	39	5.4	5.4	11.0	14.0	17.3	22.3	31.3	40.1	15.4	14.0
Yili River (C13)	Top	35	6.3	7.5	9.6	13.1	20.2	27.7	46.6	54.7	17.1	14.7
	Deep	35	3.6	4.6	7.3	8.9	13.6	19.8	26.6	26.8	11.4	10.0
Yuanjiang–Honghe River (C14)	Top	29	8.5	15.5	31.0	43.0	75.0	141	188	195	68.7	52.0
	Deep	29	8.5	10.3	30.0	43.0	79.0	126	235	347	69.4	48.3
Hainan Island River (C15)	Top	26	7.5	8.8	18.1	27.8	42.0	44.1	168	323	40.6	27.5
	Deep	26	4.5	6.1	12.3	23.5	33.5	45.5	87.1	109	28.8	21.7
Luanhe River (C16)	Top	26	6.0	8.5	13.4	22.0	39.6	53.5	175	316	39.6	25.5
	Deep	26	6.0	6.3	10.9	16.8	21.3	25.3	35.4	47.0	17.2	15.1
South-eastern Guangxi River (C17)	Top	20	20.5	23.0	41.5	70.8	99.3	108	166	178	75.9	64.8
	Deep	20	14.5	18.1	32.0	38.8	49.4	55.6	186	235	52.9	42.5
Western Liaoning River (C18)	Top	19	12.0	12.2	20.0	29.5	45.8	66.3	244	365	52.8	33.7
	Deep	19	8.0	8.7	11.5	19.0	32.0	40.1	52.0	54.5	23.8	20.0
Yalvjiang River (C19)	Top	16	18.5	21.5	39.5	64.8	134	275	356	402	116	74.5
	Deep	16	13.5	13.7	16.5	21.5	30.6	43.0	46.8	47.0	26.0	23.8
Liaodong Peninsula River (C20)	Top	14	9.0	9.5	17.4	22.0	29.9	48.5	113	121	34.7	25.9
	Deep	14	5.5	6.3	12.0	16.0	21.1	27.5	35.4	39.0	17.9	15.9
Singe–Zangpu River (C21)	Top	13	10.7	11.2	16.3	18.3	31.1	37.5	280	380	50.5	26.1
	Deep	13	10.7	11.0	14.9	16.3	30.6	37.6	159	207	35.7	22.9
Dulongjiang River (C22)	Top	8	13.5	14.4	22.3	31.8	43.8	74.0	114	122	43.7	34.1
	Deep	8	10.5	11.6	17.8	20.8	26.3	31.2	35.2	36.0	22.4	21.0
Tumenjiang River (C23)	Top	8	12.0	13.1	19.5	33.0	54.8	70.9	95.1	100	42.1	33.5
	Deep	8	8.5	8.6	15.4	20.8	24.6	26.4	29.0	29.5	19.6	17.9
Suifenhe River (C24)	Top	3	8.5	8.9	12.3	16.0	16.5	16.7	17.0	17.0	13.8	13.2
	Deep	3	8.5	8.8	11.3	14.0	26.0	30.8	36.8	38.0	20.2	16.5
Tarim Endorheic Basin (C25)	Top	330	0.5	4.6	8.4	13.1	21.2	30.7	66.1	363	19.3	14.1
	Deep	330	0.5	3.8	6.9	10.5	15.3	19.2	43.5	128	13.8	10.9
Junggar Endorheic Basin (C26)	Top	198	2.0	3.7	9.8	15.9	23.8	28.6	76.8	2246	31.1	15.6
	Deep	198	2.0	3.5	7.2	11.3	17.3	20.4	53.2	583	17.0	11.4
Hexi Corrido–Alxa endorheic basin (C27)	Top	180	4.1	5.0	8.0	11.0	19.9	31.2	83.4	211	19.9	13.5
	Deep	180	4.5	5.0	7.0	9.3	14.0	19.1	38.1	138	13.4	10.7
Inner Mongolia Endorheic Basin (C28)	Top	129	4.0	5.0	8.0	10.5	16.0	20.0	38.9	221	16.2	12.1
	Deep	128	4.0	4.5	7.0	9.5	13.6	17.5	56.2	91.0	12.9	10.4
Qiangtang Plateau Endorheic Basin (C29)	Top	124	4.6	6.1	10.6	14.8	25.0	29.6	92.5	141	23.3	17.5
	Deep	124	5.5	6.5	9.9	14.9	22.7	26.6	105	277	22.7	16.2
Qaidam Endorheic Basin (C30)	Top	101	5.1	5.1	8.7	12.3	16.4	18.6	38.5	69.9	14.2	12.3
	Deep	101	3.2	4.6	7.8	11.3	15.4	18.0	35.9	69.4	13.6	11.6
Irtysh Endorheic Basin (C31)	Top	26	3.6	3.9	5.8	10.5	15.3	15.5	28.4	33.9	11.3	9.5
	Deep	26	3.1	3.4	4.1	5.6	8.8	11.9	28.4	33.9	8.2	6.5
Erdos Endorheic Basin (C32)	Top	12	7.0	7.3	10.8	12.5	13.6	14.5	15.9	16.0	12.1	11.7
	Deep	12	4.5	5.2	8.0	9.3	12.1	13.9	17.4	18.5	10.3	9.7

Bold data shows values are significantly higher than median of whole China.

and quartz-rich windblown sand cover. Mercury is also greatly enriched in the Southern China Orogenic Belt, while there is a slight enrichment in the Songpan–Ganzi Orogenic Belt (V). The Tarim Craton (III) and Tianshan–Xingmeng Orogenic Belt (I) are depleted in Hg compared to the median value for whole China in both top and deep samples.

3.4. Mercury distribution in relation to China's geomorphological landscapes

The territory of China lies between latitudes 18° and 54° N, and longitudes 73° and 135° E. China's landscapes vary significantly across its vast width as shown in Fig. 8. In the east and north-east, there are hilly or low mountainous areas, alluvial plains, and forested land. Northern and north-western China is dominated by arid desert terrains including desert basins, Gobi desert, semi-desert grassland and loess plateaus. South-western China is dominated by high mountains, most notably the Himalayas. Table 7 lists Hg statistical parameters for top and deep samples of these 10 landscapes, and Fig. 9 displays their statistical variation in the form of boxplots. The Karst terrain (D) has the highest Hg median values among these landscapes in both top and deep samples, and the Basin desert terrain the lowest. The high Hg values in the Karst terrain are due to heavy metals enriched in red earth and laterite during the process of chemical decomposition of carbonates, and low-temperature mineralisation of Hg, Sb, As, Au and Pb–Zn. The lowest Hg values in the basin desert are because of the quartz-rich windblown sand unpolluted or slightly polluted by human activities.

3.5. Mercury distribution in China's major drainage basins

Fig. 10 shows 32 major drainage basins (C_1–C_{32}) in China. Table 8 lists Hg statistical parameters for top and deep samples of 32 basins, and Fig. 11 shows their variation in the form of boxplots. High Hg median concentrations occur in the Pearl River (C4), Yangtze River (C1) and South-eastern Coast River (C7) basins, which have the highest population density and the most industrial development in China. Low median concentrations are observed in endorheic basins of northern China due to the presence of quartz-rich windblown sand and relatively low influence from human activities, e.g., Tarim (C25), Junggar (C26), Hexi Corrido–Alxa (C27), Inner Mongolia (C28), Qiangtang Plateau (C29), Qaidan (C30), Irtysh (C31) and Erdos (C32).

3.6. Mercury distribution in relation to soil types

Fig. 12 shows the distribution of major soil types in China. Table 9 lists the summary statistical results of Hg concentrations of top and deep sediment/alluvial soil samples in regions with different soil types, and Fig. 13 presents their statistical variation in the form of boxplots. The median value varies from 11.3 to 79 μg/kg for top samples, and from 9.6 to 51.0 μg/kg for deep sediment/alluvial soil samples. The boxplots indicate the presence of a limited number of lower outliers in top and deep sediment/soil samples, while there is a considerable number of upper outliers in both cases. Statistical results show that Hg is enriched in red earth (IE) and lateritic red earth (IF) in both top and deep sediment/alluvial soil samples, and depleted in Alpine–Subalpine meadow soil (IID), Alpine desert soil (IIIA) and Grey desert soil (IIC).

Generally, the content of Hg in soil depends on the available sources and its chemical behaviour. The chemical behaviour of Hg that determines its binding ability in soil depends highly on the species, which is a function of several soil parameters, such as temperature, organic matter, clay and colloids (Kabata-Pendias and Mukherjee, 2007; Schuster, 1991; Yin et al., 1997). Red earth in southern China has a high content of clay and oxides and is low in organic matter (Fig. 4). Hence, enrichment of Hg in red earth (IE, Fig. 13) and lateritic red earth (IF) is possibly due to its absorption by clay and oxide colloids. While depletion of Hg occurs in areas with Alpine–Subalpine meadow soil (IIIC, Fig. 13), Alpine desert soil (IIIA), Grey desert soil and in Gobi desert (IIC) is due to the quartz-rich windblown sand containing low content of organic matter, clay and colloids, and in the north and north-west of China, where there is low or no pollution by human activities.

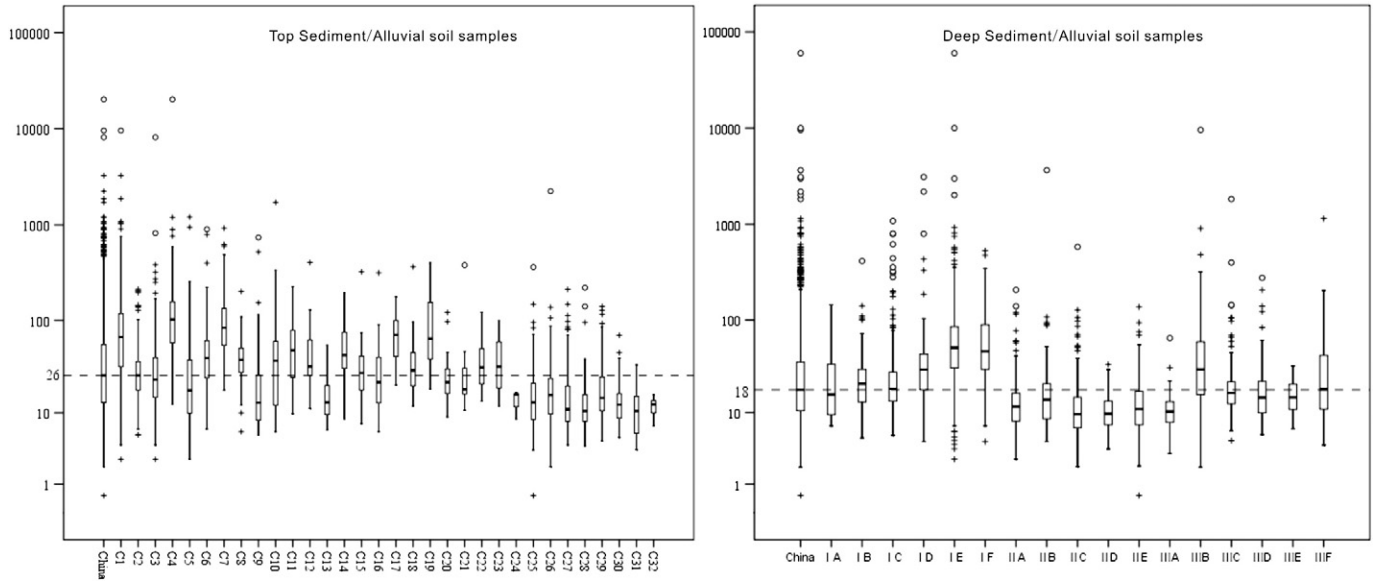

Fig. 11. Boxplots showing statistical Hg (μg/kg) variation in samples from major drainage basins of China (for boxplot characteristics see Fig. 7, and for summary statistics refer to Table 9). Notation: China — All samples; (C1) Yangtze River; (C2) Heilongjiang River; (C3) Yellow River; (C4) Pearl River; (C5) Yarlung Zangbo River; (C6) Haihe River; (C7) South-eastern Coast River; (C8) Huaihe River; (C9) Liaohe River; (C10); Lancangjiang River; (C11) Nujiang River; (C12) Shandong Peninsula River; (C13) Yili River; (C14) Yuanjiang–Honghe River; (C15) Hainan Island River; (C16) Luanhe River; (C17) South-eastern Guangxi River; (C18) Western Liaoning River; (C19) Yalvjiang River; (C20) Liaodong Peninsula River; (C21) Singe–Zangpu River; (C22) Dulongjiang River; (C23) Tumenjiang River; (C24) Suifenhe River; (C25) Tarim Endorheic Basin; (C26) Junggar Endorheic Basin; (C27) Hexi Corrido–Alxa endorheic basin; (C28) Inner Mongolia Endorheic Basin; (C29) Qiangtang Plateau Endorheic Basin; (C30) Qaidam Endorheic Basin; (C31) Irtysh Endorheic Basin; (C32) Erdos Endorheic Basin.

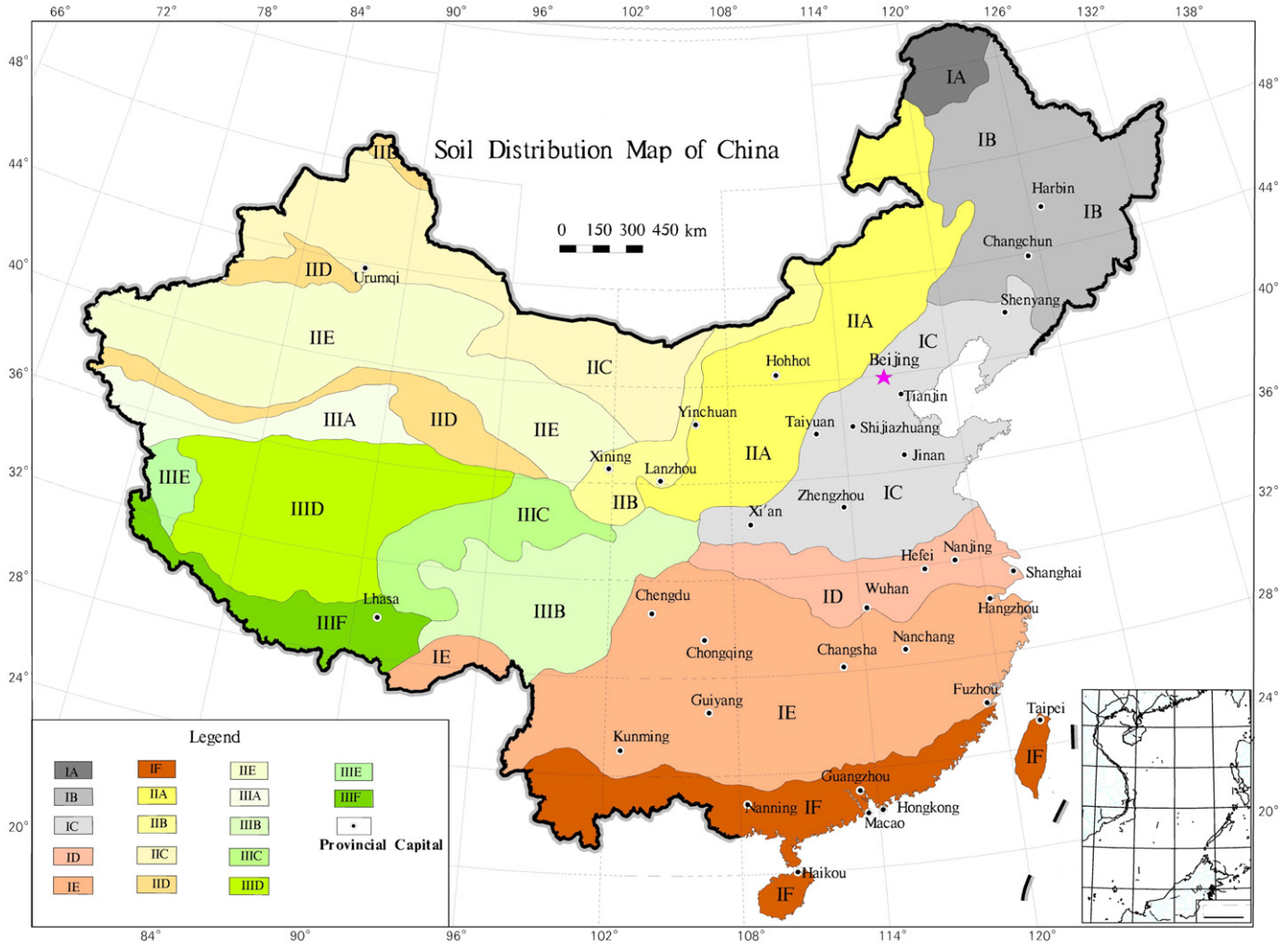

Fig. 12. Soil type distribution in China (for legend refer to Table 9 and Fig. 13).
Modified from Wang and Zuo (2010).

4. Conclusions

The China Geochemical Baselines Project, based on catchment sediment/alluvial soil sampling, provides an insight into the distribution of Hg throughout China. The data set can be used to establish Hg baselines for the major tectonic units in China, the different geomorphological landscapes, major drainage basins, and different soil types. The 25th, 50th, 75th and 85th percentiles of Hg concentrations display well the relationship of spatial distribution with lithology, mineral resources, soil types, and human activities.

The 95% range (P2.5–P97.5) varies from 5 to 281 μg/kg in top and 5 to 185 μg/kg in deep sediment/alluvial soil samples. The median Hg in top and deep sediment/alluvial soil samples is 26 and 18 μg/kg, respectively. Notable Hg enrichment occurs in top sediment/alluvial soil samples.

The overall spatial distribution patterns of Hg in both top and deep sediment/alluvial soil samples show an increasing trend from north to south and from west to east China. The areas most highly enriched in Hg mainly occur in south and south-east China, where they are primarily related to (1) the extensive distribution of black shale in south-eastern China; (2) large-scale epithermal metallogenic domain in south-western China, characterised by mineralisation of Hg, Sb, Au, As, and Pb–Zn; (3) soil type distribution from arid quartz-rich wind-blown sand or loess in the north and north-west to red earth and laterite in south, south-east and organic soil in north-east, and (4) population density and economic development from low in north-west to high in south-east China.

The spatial distribution map of Hg ratios of top to deep sediment/alluvial soil samples better visualises the influence of human activities in the top samples in the highly populated urban areas of eastern China, such as at the Yangtze River Delta (Shanghai-Jiangsu-Zhejiang), the Pearl River Delta (Guangzhou) and North China Plains (Beijing–Tianjin–Shijiazhuang–Taiyuan). The higher ratios of top to deep sediment/alluvial soil in these areas are mainly caused by Hg emissions from metal smelting, coal combustion, and battery, fluorescent lamp, thermometer and cement production activities. A proportion of 6.86% top and 3.52% deep sediment/alluvial soil sample sites have Hg concentrations higher than the soil contamination limit of 150 μg/kg set by the National Environmental Standards for Heavy Metals of the People's Republic of China.

Acknowledgements

Many thanks are given to all participants in the China Geochemical Baselines project. The authors thank EurGeol Alecos Demetriades for his comments on the original manuscript and language revision, and Dr. David Smith for the thorough review and suggestions for the improvement of the manuscript. This research was financially supported by 'Sino-probe 04-01 (201011053)'.

Table 9
Statistical parameters of Hg analytical results (μg/kg) in top and deep sediment/alluvial soil samples in the areas of different soil types of China (see also Fig. 13).

Soil type	Sample type	N	Percentile								Mean	Geometric Mean
			Min.	2.5%	25%	50%	75%	85%	97.5%	Max.		
Whole China	Top	3382	0.5	5.2	13.1	26.0	55.5	86.9	279	20,201	67.0	28.7
	Deep	3380	0.5	4.6	10.5	18.0	36.0	55.2	188	60,001	64.8	21.0
Cryo-brown soil–Podsolic soil (IA)	Top	35	11.0	11.9	20.3	36.0	42.0	54.9	93.4	144	38.4	32.2
	Deep	35	7.0	7.4	9.5	16.0	34.3	47.8	81.2	145	28.0	20.2
Dark brown forest soil–Black soil (IB)	Top	296	5.5	7.2	18.0	26.5	38.1	44.5	133	402	34.9	26.5
	Deep	295	5.0	6.0	13.3	21.0	30.0	35.5	65.3	416	25.1	19.8
Brown forest soil–Cinnamon soil (IC)	Top	333	6.5	11.3	26.0	38.5	62.5	85.8	351	1086	64.0	42.5
	Deep	333	5.4	7.0	13.5	18.5	28.0	34.0	258	1086	38.7	21.3
Yellow-brown earth, Yellow-cinnamon soil (ID)	Top	124	6.0	14.7	37.5	53.0	79.5	102	373	1876	93.9	57.7
	Deep	124	4.5	8.3	18.0	29.9	43.8	53.8	426	3121	87.8	31.7
Red earth–Yellow earth (IE)	Top	575	2.6	9.0	45.0	79.0	131	183	565	20,201	157	77.3
	Deep	575	2.6	10.1	31.0	51.0	85.3	116	351	60,001	205	53.8
Lateritic red earth (IF)	Top	204	7.5	12.5	38.5	74.0	129	166	323	891	100	69.8
	Deep	204	4.5	9.5	30.0	46.8	89.5	119	261	531	69.5	49.1
Chernozem-Chestnut soil–loessial soil (IIA)	Top	360	2.6	5.0	10.0	15.0	23.5	27.5	99.9	901	25.3	15.9
	Deep	360	2.6	4.1	8.0	11.7	16.5	21.5	42.1	208	15.3	12.2
Sierozem-Brown soil (IIB)	Top	90	5.5	5.5	10.0	14.3	26.3	39.1	107	8125	114	18.0
	Deep	89	4.5	4.5	8.5	14.0	21.0	27.0	93.6	3670	60.2	15.1
Grey desert soil (IIC)	Top	356	2.0	4.1	8.0	12.9	21.5	28.1	84.1	2246	25.8	13.9
	Deep	356	2.0	3.6	6.6	9.6	14.9	19.3	51.6	583	14.8	10.4
Alpine–Subalpine meadow soil (IID)	Top	119	5.1	5.1	7.9	11.3	15.4	19.1	34.3	45.1	13.3	11.7
	Deep	119	3.7	4.5	7.2	9.7	13.5	15.9	26.9	33.9	11.1	10.0
Alpine brown soil–Chestnut soil (IIE)	Top	338	0.5	4.6	8.9	14.5	25.0	34.6	67.9	211	20.3	15.1
	Deep	338	0.5	4.1	7.3	11.0	17.3	21.5	43.0	138	14.7	11.6
Alpine desert soil (IIIA)	Top	49	4.7	5.8	9.3	11.8	14.4	16.3	43.5	51.7	13.5	12.0
	Deep	49	3.2	4.3	7.8	10.3	13.4	15.1	29.6	64.7	12.0	10.2
Subalpine meadow soil (IIIB)	Top	193	2.7	4.6	20.0	34.5	59.5	97.1	276	9550	118	36.4
	Deep	193	2.0	4.0	16.0	30.0	59.1	91.5	288	9550	105	32.1
Alpine meadow soil (IIIC)	Top	84	6.7	9.9	14.2	18.5	28.3	45.9	168	1208	44.8	22.8
	Deep	84	4.6	7.2	12.8	16.6	22.0	35.2	144	1835	51.1	20.5
Alpine steppe soil (IIID)	Top	120	4.6	6.0	10.7	14.4	22.9	28.6	116	380	24.2	16.9
	Deep	120	5.5	6.5	9.9	14.8	22.1	25.7	123	277	22.8	16.1
Subalpine desert soil (IIIE)	Top	18	7.0	8.0	10.5	16.6	22.3	26.2	34.5	37.0	17.4	15.7
	Deep	18	6.5	6.5	11.2	14.9	19.9	21.7	31.5	32.5	15.9	14.4
Subalpine steppe soil (IIIF)	Top	88	3.6	4.6	11.7	18.8	40.6	68.3	179	948	44.8	22.9
	Deep	88	4.1	4.6	11.1	18.3	42.4	53.0	177	1147	45.7	22.2

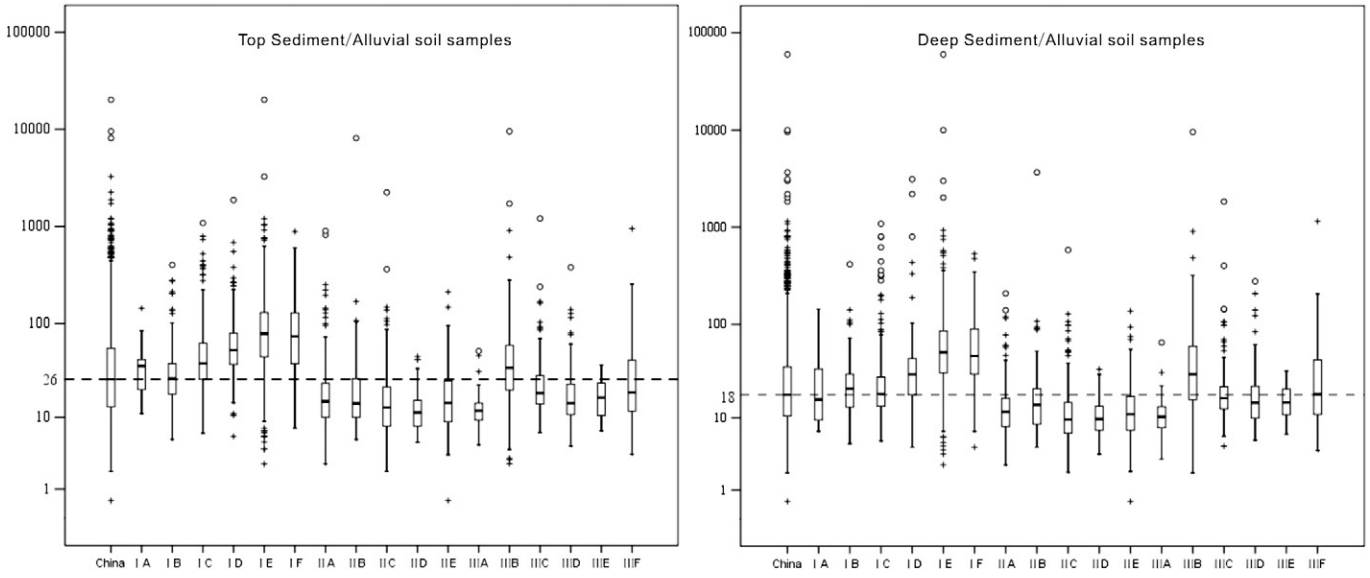

Fig. 13. Boxplots displaying statistical Hg (μg/kg) variation of top and deep sediment/alluvial soil samples in the areas of different soil types of China (for boxplot characteristics see Fig. 7, and for summary statistics refer to Table 9). Notation: China — All samples; (IA) Cryo-brown soil–Podsolic soil; (IB) Dark brown forest soil–Black soil; (IC) Brown forest soil–Cinnamon soil; (ID) Yellow-brown earth, Yellow-cinnamon soil; (IE) Red earth–Yellow earth; (IF) Lateritic red earth. (IIA) Chernozem-Chestnut soil–loessial soil; (IIB) Sierozem-Brown soil; (IIC) Grey desert soil; (IID) Alpine–Subalpine meadow soil; (IIE) Alpine brown soil–Chestnut soil; (IIIA) Alpine desert soil; (IIIB) Subalpine meadow soil; (IIIC) Alpine meadow soil; (IIID) Alpine steppe soil; (IIIE) Subalpine desert soil (IIIF) Subalpine steppe soil.

References

Chi, Qinghua, Yan, Mingcai, 2007. Handbook of Elemental Abundance for Applied Geochemistry. Geological Publishing House, Beijing, China (148 pp.).

Clarke, F.W., Washington, H.S., 1924. The composition of the Earth's Crust. U. S. Geol. Surv. Prof. Pap. 127 (117 pp., http://pubs.usgs.gov/pp/0127/report.pdf).

Coveney Jr., R.M., Chen, N.S., 1991. Ni–Mo–PGE–Au rich ores in Chinese black shales and speculations on possible analogues in the United States. Mineral. Deposita 26, 83–88.

Darnley, A.G., Björklund, A., Bølviken, B., Gustavsson, N., Koval, P.V., Plant, J.A., Steenfelt, A., Tauchid, M., Xuejing, X., Garrett, R.G., Hall, G.E.M., 1995. A global geochemical database for environmental and resource management: final report of IGCP Project 259. Earth Sciences 19. UNESCO Publishing, Paris (122 pp., http://www.globalgeochemicalbaselines.eu/wp-content/uploads/2012/07/Blue_Book_GGD_IGCP259.pdf).

De Vos, W., Tarvainen, T. (Chief Editors), Salminen, R., Reeder, S., De Vivo, B., Demetriades, A., Pirc, S., Batista, M.J., Marsina, K., Ottesen, R.T., O'Connor, P.J., Bidovec, M., Lima, A., Siewers, U., Smith, B., Taylor, H., Shaw, R., Salpeteur, I., Gregorauskiene, V., Halamic, J., Slaninka, I., Lax, K., Gravesen, P., Birke, M., Breward, N., Ander, E.L., Jordan, G., Duris, M., Klein, P., Locutura, J., Bel-lan, A., Pasieczna, A., Lis, J., Mazreku, A., Gilucis, A., Heitzmann, P., Klaver, G., Petersell, V., 2006. Geochemical atlas of Europe. Part 2 — interpretation of geochemical maps, additional tables, figures, maps, and related publications. Geological Survey of Finland, Espoo, 692 pp., http://weppi.gtk.fi/publ/foregsatlas/.

Dong, Shuwen, Li, Tingdong, 2009. SinoProbe: the exploration of the deep interior beneath the Chinese continent. Acta Geol. Sin. 83, 895–909 (in Chinese with English abstract).

Fitzgerard, W.F., Lamborg, C.H., 2003. Geochemistry of mercury in the environment. Chapter 9 In: Lollar, B.S. (Ed.), Environmental Geochemistry. Volume 9 In: Holland, H.D., Turekian, K.K. (Exec. Eds.), Treatise on Geochemistry. Elsevier Ltd., 108–148.

Fitzgerard, W.F., Lamborg, C.H., 2014. Geochemistry of mercury in the environment. Chapter 11.4 In: Lollar, B.S. (Ed.), Environmental Geochemistry. Volume 11 In: Holland, H.D., Turekian, K.K. (Eds.-in-Chief), Treatise on Geochemistry. Elsevier Ltd., 91–129.

Gao, Shan, Tingchuan, Luo, Benren, Zhang, Hongfei, Zhang, Yinwen, Han, Zhidan, Zhao, Yiken, Hu, 1998. Chemical composition of the continental crust as revealed by studies in East China. Geochim. Cosmochim. Acta 62, 1959–1975.

Gao, Shan, Tingchuan, Luo, Benren, Zhang, Hongfei, Zhang, YInwen, Han, Zhidan, Zhao, Kern, H., 1999. Crustal and composition of Eastern China. Sci. Sin. (D) 29, 204–213.

Goldschmidt, V.M., 1954. Geochemistry. Clarendon Press, Oxford (730 pp.).

Gunson, A.J., Viega, M.M., 2004. Mercury and artisanal mining in China. Environ. Pract. 6 (2), 109–120.

Gunson, A.J., Yue, Jian, 2001. Artisanal mining in the People's Republic of China. Report No. 74, Mining, minerals and sustainable development project. International Institute for Environment and Development, London, UK (19 pp.).

Harris, N.B.W., Xu, R., Lewis, C.L., 1988. Isotope geochemistry of the 1985 Tibet Geotraverse, Lhasa to Golmud. Philos. Trans. R. Soc. Lond. Ser. A 327, 263–285.

Harris, N.B.W., Inger, S., Ronghua, X., 1990. Cretaceous plutonism in Central Tibet: an example of postcollision magmatism. J. Volcanol. Geotherm. Res. 44 (1–2), 21–32.

Hu, Ruizhong, Su, Wenchao, Bi, Xianwu, Tu, Guangzhi, Hofstra, Albert H., 2002. Geology and geochemistry of Carlin-type gold deposits in China. Mineral. Deposita 37, 378–392.

Hu, Ruizhong, Peng, Jiantang, Ma, Dongsheng, Su, Wenchao, Shi, Chuanhua, Bi, Xianwu, 2007. Epoch of large-scale low temperature mineralizations in southwestern Yangtze massif. Mineral Deposits 26 (6), 583–596 (in Chinese with English abstract).

Huang, Zhilong, Hu, Ruizhong, Su, Wenchao, Wen, Hanjie, Liu, Shen, Fu, Yazhou, 2011. A study on the large-scale low temperature metallogenic domain in southwestern China—significance, history and new progress. Acta Mineral. Sin. 31 (3), 309–314 (in Chinese with English abstract).

Japan Environmental Agency, 1989. Quality of the Environment in Japan—1989. pp. 242–243 (Tokyo).

Kabata-Pendias, A., Mukherjee, A.B., 2007. Trace Elements from Soil to Human. Springer-Verlag, Berlin (550 pp.).

Kapp, P., Murphy, M.A., Yin, A., Harrison, M., 2003. Mesozoic and Cenozoic tectonic evolution of the Shiquanhe area of western Tibet. Tectonics 22, 4-1-9.

Kürzl, H., 1988. Exploratory data analysis: recent advances for the interpretation of geochemical data. J. Geochem. Explor. 30 (3), 309–322.

Li, H.Y., 2012. Destruction of North China Craton: insights from temporal and spatial evolution of the proto-basins and magmatism. Sci. China Ser. D Earth Sci. 9, 1–15.

Lin, Yuhuan, Guo, Mingxin, Gan, Weiming, 1997. Mercury pollution from small gold mines in China. Water Air Soil Pollut. 97, 233–239.

Mao, Jingwen, Lehmann, Bernd, Du, Andao, Zhang, Guangdi, Ma, Dongsheng, Wang, Yitian, Zeng, Mingguo, Kerrich, Robert, 2002. Re–Os dating of polymetallic Ni–Mo–PGE–Au mineralization in Lower Cambrian black shales of South China and its geologic significance. Econ. Geol. 97, 1051–1061.

Miao, L.C., Liu, D.Y., Zhang, F.Q., 2007. Zircon SHRIMP U–Pb ages of the Xinghuadukou Group in Hanjiayuanzi and Xinlin areas and the Zhalantun Group in Inner Mongolia, Da Hinggan Mountains. Chin. Sci. Bull. 52, 1112–1134.

Ottesen, R.T., Birke, M., Finne, T.E., Gosar, M., Locutura, J., Reimann, C., Tarvainen, T., the GEMAS Project Team, 2013. Mercury in European agricultural and grazing land soils. Appl. Geochem. 33, 1–12.

Parker, R., 1967. Composition of the Earth's Crust. Chapter D In: Fleischer, M. (Techn. Ed.), Data of Geochemistry, Sixth Edition. U.S. Geological Survey Professional Paper 440-D. United States Government Printing Office, Washington, 17 pp., http://pubs.usgs.gov/pp/0440d/report.pdf

Pirajno, F., 2013. The Geology and Tectonic Settings of China's Mineral Deposits. Springer, Dordrecht Heidelberg London New York (222 pp.).

Qiu, Guangle, Feng, Xinbin, Wang, Shaofeng, Xiao, Tangfu, 2006. Mercury contaminations from historic mining to water, soil and vegetation in Lanmuchang, Guizhou, southwestern China. Sci. Total Environ. 368, 56–68.

Ren, J.S., Wang, Z.X., Chen, B.W., Jiang, C.F., Niu, B.G., Li, J.Y., Xie, G.L., He, Z.J., Liu, Z.G., 1999. The Tectonics of China from a Global View—A Guide to the Tectonic Map of China and Adjacent Regions. Geological Publishing House, Beijing (32 pp.).

Schuster, E., 1991. The behavior of mercury in the soil with special emphasis on complexation and adsorption processes: a review of the literature. Water Air Soil Pollut. 56, 667–680.

Şengör, A.M.C., Natal'in, B.A., Burtman, U.S., 1993. Evolution of the Altaid tectonic collage and Paleozoic crustal growth in Eurasia. Nature 364, 209–307.

Shaw, D.M., Cramer, J.J., Higgins, M.D., Truscott, M.G., 1986. Composition of the Canadian Precambrian shield and the continental crust of the Earth. In: Dawson, J.B., Carswell, D.A., Hall, J., Wedepohl, K.H. (Eds.), The Nature of the Lower Continental Crust. Geological Society of London, Special Publication 24, pp. 257–282.

Smith, D.B., Xueqiu, Wang, Reeder, S., Demetriades, A., 2012. The IUGS/IAGC task group on global geochemical baselines. Earth Sci. Front. 19 (30), 1–6.

Song, S.G., Zhang, L.F., Niu, Y.L., Su, L., Song, B., Liu, D.Y., 2006. Evolution from oceanic subduction to continental collision: a case study from the Northern Tibetan Plateau based on geochemical and geochronological data. J. Petrol. 47, 435–455.

Streets, G.D., Hao Jiming, Wu., Ye, Jiang Jingkun, Chan, M., Hezhong, Tian, Xinbin, Feng, 2005. Anthropogenic mercury emissions in China. Atmos. Environ. 39, 7789–7806.

Taylor, S.R., 1964. The abundance of chemical elements in the continental crust: a new table. Geochim. Cosmochim. Acta 28, 1273–1285.

Tukey, J.W., 1977. Exploratory Data Analysis. Addison-Wesley, Reading, Massachusetts (506 pp.).

USEPA (U.S. Environmental Protection Agency), 1997. Mercury Study Report to Congress—An Assessment of Exposure to Mercury in the United States. EPA-452/R-97-006 (http://www.epa.gov/ttn/oarpg/t3/reports/volume4.pdf).

Vinogradov, A.P., 1962. Average concentration of chemical elements in the chief types of igneous rocks of crust of the earth. Geokhimiya 7, 641–664 (in Russian).

Wang, Z.H., 2004. Tectonic evolution of the western Kunlun orogenic belt, western China. J. Asian Earth Sci. 24, 153–161.

Wang, Xueqiu, 2012. Global geochemical baselines: understanding the past and predicting the future. Earth Sci. Front. 19 (3), 7–18 (in Chinese with English abstract).

Wang, Xueqiu, the CGB Sampling Team, 2015. China geochemical baselines: sampling methodology. In: Demetriades, A., Birke, M., Albanese, S., Schoeters, I., De Vivo, B. (Eds.), Continental, Regional and Local Scale Geochemical Mapping, Special Issue. Journal of Geochemical Exploration 148, pp. 25–39 (in this issue).

Wang, Jingan, Zuo, Wei (Eds.), 2010. Geographic Atlas of China. SinoMaps, Beijing (362 pp.).

Wang, Q., Wyman, D.A., Zhu, Y.T., Zhao, Z.H., 2008. Late Triassic rhyolites and high-Mg andesites in the northern Hohxil area, Songpan–Ganzi terrane. Goldschmidt Conference Abstract, A999.

Wang, Xueqiu, Xie, Xuejing, Zhang, Benren, Zhang, Qin, Chi, Qinghua, Hou, Qingye, Xu, Shanfa, Zhang, Bimin, 2010. China geochemical probe: making "geochemical earth". Acta Geol. Sin. 84 (6), 854–864 (in Chinese with English abstract).

Wedepohl, K.H., 1995. The composition of the continental crust. Geochim. Cosmochim. Acta 59, 1217–1232.

Wu, F.Y., Sun, D.Y., Li, H.M., Wang, X.L., 2001. The nature of basement beneath the Songliao Basin in NE China: geochemical and isotopic constraints. Phys. Chem. Earth Solid Earth Geod. 26, 793–803.

Wu, Ye, Wang, Shuxiao, Streets, G.D., Hao, Jiming, Chan, Melissa, Jiang, Jingkun, 2006. Trends in anthropogenic mercury emissions in China from 1995 to 2003. Environ. Sci. Technol. 40, 5312–5318.

Wu, F.Y., Yang, J.H., Lo, C.H., Wilde, S.A., Sun, D.Y., Jahn, B.M., 2007. The Heilongjiang group: a Jurassic accretionary complex in the Jiamusi Massif at the western Pacific margin of northeastern China. Island Arc 16, 156–172.

Xie, Xuejing, Yan, Mingcai, Li, Lianzhong, Shen, Huijun, 1985. Usable values for Chinese standard reference samples of stream sediment, soil and rocks GSD 9–12, GSS 1–8 and GSR 1–6. Geostand. Newslett. 9 (2), 227–280.

Xu, R.H., Scharer, U., Allègre, C.J., 1985. Magmatism and metamorphism in the Lhasa block (Tibet): a geochronological study. J. Geol. 93, 41–57.

Xu, R.H., Zhang, Y.Q., Xie, Y.W., Vadal, P., Nicolas, A., Zhang, Q.D., Zhao, D.M., 1996. Isotopic geochemistry of plutonic rocks. In: Pan, Y.S. (Ed.), Geologic Evolution of the Karakorum and Kunlun Mountains. Seismological Press, Beijing, pp. 137–186.

Xu, Y.G., He, B., Chung, S.L., Menzies, M.A., Frey, F.A., 2004. The geologic, geochemical and geophysical consequences of plume involvement in the Emeishan flood basalt province. Geology 30, 917–920.

Yan, Mingcai, Chi, Qinghua, 1997. Crustal abundance and distribution of the chemical elements in the North China Platform. In: Xie, Xuejing (Ed.), Geochemistry. Proceedings 30th International Geological Congress 19. International Science Publishers, Amsterdam, pp. 65–81.

Yin, A., Harrison, T.M., 2000. Geologic evolution of the Himalaya–Tibetan Orogen. Annu. Rev. Earth Planet. Sci. 28, 211–280.

Yin, Y., Allen, E., Huang, C.P., Sanders, P.F., 1997. Adsorption/desorption isotherms of Hg (II) by soil. Soil Sci. 162, 35–45.

Zhang, L., Wong, M.H., 2007. Environmental mercury contamination in China, source and impacts. Environ. Int. 33, 108–121.

Zhang, Jinmao, Zhang, Qin, 1986. Determination of micro amount of Hg in geological samples by cold atomic-non-dispersive atomic fluorescence spectrometric method. Anal. Miner. Rocks 1, 37–41.

Zhang, J.H., Ge, W.C., Wu, F.Y., Wilde, S.A., Yang, J.H., Liu, X.M., 2008. Large-scale Early Cretaceous volcanic events in the northern Great Xing'an Range, Northeastern China. Lithos 102, 138–157.

Zhang, J.H., Gao, S., Ge, W.C., Wu, F.Y., Yang, J.H., Wilde, S.A., Li, M., 2010. Geochronology of the Mesozoic volcanic rocks in the Great Xing'an Range, northeastern China: implications for subduction-induced delamination. Chem. Geol. 276, 144–165.
Zhang, Qin, Bai, Jinfeng, Wang, Ye, 2012. Analytical scheme and quality monitoring system for China Geochemical Baselines. Earth Sci. Front. 19 (3), 33–42 (in Chinese with English abstract).
Zhao, G.C., Sun, M., Wilde, S.A., 2003. Major tectonic units of the North China Craton and their Paleoproterozoic assembly. Sci. China Ser. D Earth Sci. 46, 23–38.
Zheng, Y.F., Xiao, W.J., Zhao, G.C., 2013. Introduction to tectonics of China. Gondwana Res. 23, 1189–1206.
Zhu, D.C., Zhao, Z.D., Niu, Y.L., Dilek, Y., Hou, Z.Q., Mo, X.X., 2013. The origin and pre-Cenozoic evolution of the Tibetan Plateau. Gondwana Res. 23 (4), 1429–1454.